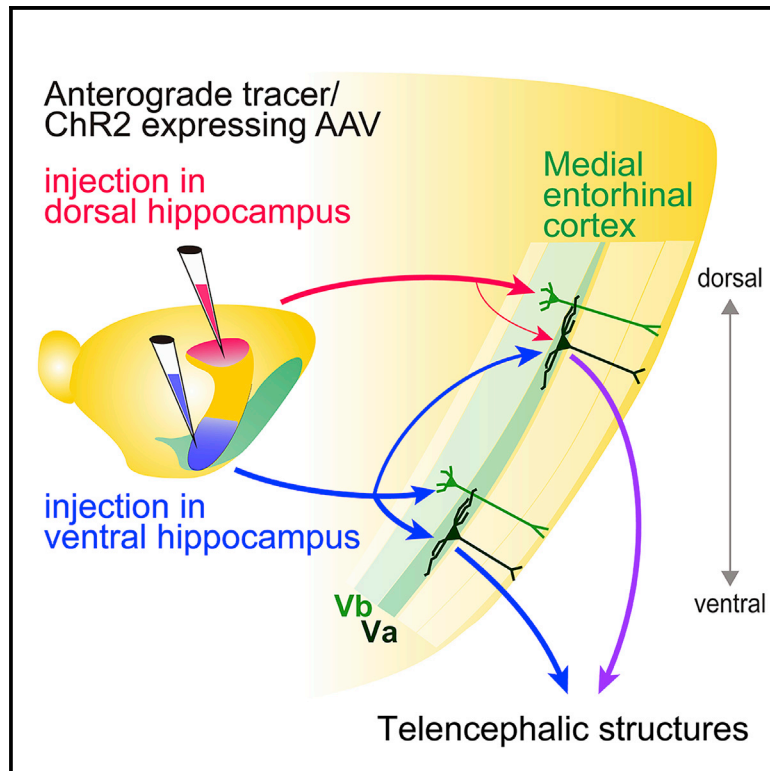# Hippocampal-medial entorhinal circuit is differently organized along the dorsoventral axis in rodents

## Graphical abstract



## Authors

Shinya Ohara, Märt Rannap,
Ken-Ichiro Tsutsui, Andreas Draguhn,
Alexei V. Egorov, Menno P. Witter

## Correspondence

alexei.egorov@urz.uni-heidelberg.de
(A.V.E.),
menno.witter@ntnu.no (M.P.W.)

## In brief

Ohara et al. have revised the organization of the canonical output circuit of the hippocampal formation to the entorhinal cortex (EC). They report that the ventral hippocampus projects broadly along the dorsoventral extent of the medial EC, mainly targeting layer Va neurons. Thus, the ventral hippocampus might control signal flow in hippocampal-neocortical circuits.

## Highlights

- Hippocampus (HS) projects topographically to LEC but not to MEC

- HS-MEC circuit exhibits a diverse connectivity pattern along the dorsoventral axis

- Dorsal HS targets dorsal MEC, while ventral HS targets both ventral and dorsal MEC

- Dorsal HS mainly targets LVb neurons, while ventral HS mainly targets LVa neurons

CellPress

## Article

# Hippocampal-medial entorhinal circuit is differently organized along the dorsoventral axis in rodents

Shinya Ohara,[1,3,4,5] Märt Rannap,[2,5] Ken-Ichiro Tsutsui,[1] Andreas Draguhn,[2] Alexei V. Egorov,[2,6,*]
and Menno P. Witter[3,6,7,*]

[1]Laboratory of Systems Neuroscience, Tohoku University Graduate School of Life Sciences, Sendai, Japan
[2]Institute of Physiology and Pathophysiology, Medical Faculty, Heidelberg University, Heidelberg, Germany
[3]Kavli Institute for Systems Neuroscience, Center for Computational Neuroscience, Egil and Pauline Braathen and Fred Kavli Center for Cortical Microcircuits, NTNU Norwegian University of Science and Technology, Trondheim, Norway
[4]PRESTO, Japan Science and Technology Agency (JST), Tokyo, Japan
[5]These authors contributed equally
[6]Senior author
[7]Lead contact
*Correspondence: alexei.egorov@urz.uni-heidelberg.de (A.V.E.), menno.witter@ntnu.no (M.P.W.)
https://doi.org/10.1016/j.celrep.2023.112001

## SUMMARY

The general understanding of hippocampal circuits is that the hippocampus and the entorhinal cortex (EC) are topographically connected through parallel identical circuits along the dorsoventral axis. Our antero-grade tracing and *in vitro* electrophysiology data, however, show a markedly different dorsoventral organization of the hippocampal projection to the medial EC (MEC). While dorsal hippocampal projections are confined to the dorsal MEC, ventral hippocampal projections innervate both dorsal and ventral MEC. Further, whereas the dorsal hippocampus preferentially targets layer Vb (LVb) neurons, the ventral hippocampus mainly targets cells in layer Va (LVa). This connectivity scheme differs from hippocampal projections to the lateral EC, which are topographically organized along the dorsoventral axis. As LVa neurons project to telencephalic structures, our findings indicate that the ventral hippocampus regulates LVa-mediated entorhinal-neocortical output from both dorsal and ventral MEC. Overall, the marked dorsoventral differences in hippocampal-entorhinal connectivity impose important constraints on signal flow in hippocampal-neocortical circuits.

## INTRODUCTION

The entorhinal cortex (EC) constitutes a major gateway between the hippocampus and the neocortex and, together with the hippocampus, plays a crucial role in episodic memory and spatial navigation. Previous studies have shown that the hippocampus is functionally differentiated along the dorsoventral axis,[1,2] which is accompanied by a functional gradient in EC.[3] This is well characterized by the change in spatial representations of hippocampal place cells and entorhinal grid cells along the dorsoventral axis in rodents: the size of place fields increases as one moves from dorsal to ventral in the hippocampus.[4,5] In parallel, the spacing between grid cell firing locations increases from dorsal to ventral in the medial EC (MEC).[6–8] In line with such functional dorsoventral gradients, the reciprocal connections between the hippocampus and EC follow a corresponding topography: the dorsal hippocampus is connected to the dorsolateral EC, whereas the ventral hippocampus is connected to the ventromedial EC.[9–14] Despite this functional topography, the connectional organization of the entorhinal-hippocampal circuit itself is

thought to be largely identical along the dorsoventral axis. Hippocampal input circuits are mediated by EC neurons in the superficial layers (layers II and III), providing inputs to all subfields of the hippocampus. In contrast, hippocampal output projections from CA1 and the subiculum terminate in the deep layers of EC (layers V and VI), which in turn project to other brain regions.[15]

In addition to recent reports in which the organization of the hippocampal input pathway has been further detailed,[16,17] the structure of the hippocampal output circuit has been extensively revised based on the finding that entorhinal layer V can be genetically divided into two sublayers: Va (LVa) and Vb (LVb).[18] The two sublayers are characterized by a distinct connectivity: LVa neurons project to telencephalic structures,[19] whereas LVb neurons project locally to superficial EC layers, forming a recurrent entorhinal-hippocampal loop.[20] It has been reported that input from the dorsal hippocampus to MEC is markedly weaker for LVa than for LVb neurons,[19,21,22] and intrinsic connections from LVb to LVa neurons in the dorsal part of MEC are sparser than in the lateral EC (LEC).[23] These findings indicate that the dorsal MEC might not convey hippocampal information to the

neocortex as effectively as LEC, challenging the current understanding on systems consolidation.[24] It further raises the questions of what the main source of inputs to LVa neurons in the dorsal MEC might be and how MEC transfers hippocampal information to the neocortex.

In a previous study,[22] we showed that CA1 projections from the intermediate hippocampus to the intermediate MEC target not only MEC-LVb but also MEC-LVa neurons. On the basis of these results, we hypothesized that hippocampal innervation of MEC-LVa might differ along the dorsoventral axis, such that dorsal MEC-LVa neurons receive hippocampal input from more intermediate and/or ventral levels of the hippocampus. In this study, using anterograde tracing and *in vitro* electrophysiology in rodents, we experimentally tested this hypothesis by examining the projections of CA1 and subiculum to MEC along the dorsoventral axis. We confirmed the previously reported topographical projections along the dorsoventral axis in the hippocampal-LEC circuit and showed that hippocampal outputs to LEC target both LVa and LVb regardless of the chosen dorsoventral level of origin. Importantly, we found that hippocampal projections to MEC differ profoundly along the dorsoventral axis: the dorsal hippocampus projects preferentially to dorsal MEC-LVb, whereas ventral hippocampal levels innervate MEC-LVa neurons in both the dorsal and the ventral MEC. This organization indicates that dorsal and ventral hippocampal levels interact differently with MEC circuits along the dorsoventral axis and that the ventral hippocampus might influence the LVa-mediated cortical output of the dorsal hippocampus.

## RESULTS

### Hippocampal-entorhinal projections along the dorsoventral axis in rats

We anatomically examined the hippocampal-entorhinal projections by injecting anterograde tracers into the output structure of the hippocampal formation, either CA1 or subiculum, at different dorsoventral and proximodistal levels. The distribution of labeled fibers in EC was first examined in the rat horizontal plane (n = 14; Figures 1, S2, and S3). In line with previous studies,[12,25] we observed a topographical organization of hippocampal-entorhinal projections along the proximodistal axis of the hippocampus. Anterograde tracer injections in dorsal-proximal CA1/distal subiculum resulted in labeled fibers mainly in the dorsal MEC, whereas injections in dorsal-distal CA1/proximal subiculum resulted in labeled fibers preferentially in the dorsolateral LEC. We also corroborated the laminar preference of hippocampal-MEC projections as previously reported,[19–22] in that labeled fibers originating from dorsal-proximal CA1 were mainly distributed in LVb of the dorsal MEC (Figure 1B). To examine the distribution of hippocampal-entorhinal projections in LVa and LVb, as well as along the dorsoventral and mediolateral extent of EC, we mapped the quantified label intensities on an unfolded EC map (Figure S1; see STAR Methods for detail). All samples with an injection either in dorsal-proximal CA1 or dorsal-distal subiculum showed preferential projections to LVb rather than LVa of the dorsal MEC, and hardly any projections to LEC (Figures 1B, 1C, and S2). This was further confirmed by quantifying the proportion of labeled fibers among all labeled fibers (Figure 1D; two-tailed paired t test, MEC-LVa vs. MEC-LVb, t4 = 4.895, **p = 0.0081; LEC-LVa vs. LEC-LVb, t4 = 0.4097, p = 0.703). The laminar preference of hippocampal-MEC projections differed when the anterograde tracer was injected into the ventral hippocampus (Figure 1A). It should be noted that in this study we use "ventral hippocampus" to denominate the ventral half of the hippocampus, including ventral and ventral-intermediate hippocampal levels. The injections into the ventral hippocampus mostly involved the ventral-intermediate level and less often the ventral pole of the hippocampus. In these cases, labeled axons in the ventral MEC were seen in LVa as well as in LVb; but at more dorsal levels, labeling was mainly present in LVa (Figures 1B, 1C, and S3). As a result, the overall distribution of ventral hippocampal axons was significantly higher in MEC-LVa than in MEC-LVb, while there were no significant differences between LEC sublayers (Figure 1D; two-tailed paired t test, MEC-LVa vs. MEC-LVb, t6 = 7.26, **p = 0.0003; LEC-LVa vs. LEC-LVb, t6 = 1.069, p = 0.3261). The ventral hippocampal projections were also characterized by their broad distribution along the dorsoventral axis of MEC, targeting not only ventral MEC but also dorsal MEC-LVa (Figures 1C, 1E, and S3). This is contrary to previous anatomical studies, which have reported that hippocampal-entorhinal projections are topographically organized along the dorsoventral axis: the dorsal hippocampus projects to the dorsal EC and the ventral hippocampus to the ventral EC.[12,13]

We next examined the hippocampal projections in rat coronal sections (n = 19; Figures 2, S4, and S5), which have been widely used in previous studies to examine hippocampal-entorhinal projections.[12,13] Samples with an injection near the border of CA1 and subiculum showed preferential projections to LEC over MEC (Figure S4), similar to what we observed in horizontal sections (Figure S2). These hippocampal-LEC projections exhibited a clear topography along the dorsoventral axis: the dorsal hippocampus projected to the dorsal (lateral) LEC, and more ventrally located parts of the hippocampus projected to more ventral (medial) locations in LEC (Figures 2B, 2C, and 2E). This topographical pattern was observed both in LEC-LVa and in LEC-LVb (Figures 2D and 2E). When the anterograde tracer was injected into either proximal CA1 or distal subiculum, labeled axons were mainly present in MEC (Figure S5). Similar to the results in horizontal sections (Figure 1), labeled axons originating from the dorsal hippocampus mainly distributed in LVb of the dorsal (posterior) MEC. In contrast, labeled axons from the ventral hippocampus distributed in LVb in the ventral (anterior) MEC and also in LVa in the dorsal (posterior) MEC (Figures S5B and S5D). However, since dorsal MEC-LVa is a thin layer running parallel to the coronal plane, the projection from the ventral hippocampus to the dorsal MEC-LVa was not as clear as in the horizontal plane. Taken together, these data indicate that the previously reported topographical organization along the dorsoventral axis applies to hippocampal-LEC projections but not to hippocampal-MEC projections. In addition, the laminar preference of hippocampal-MEC projections differs between the dorsal and the ventral hippocampus: the dorsal hippocampus preferentially targets LVb in the dorsal MEC, whereas the ventral hippocampus targets LVa in the dorsal and both LVa and LVb in the ventral MEC.
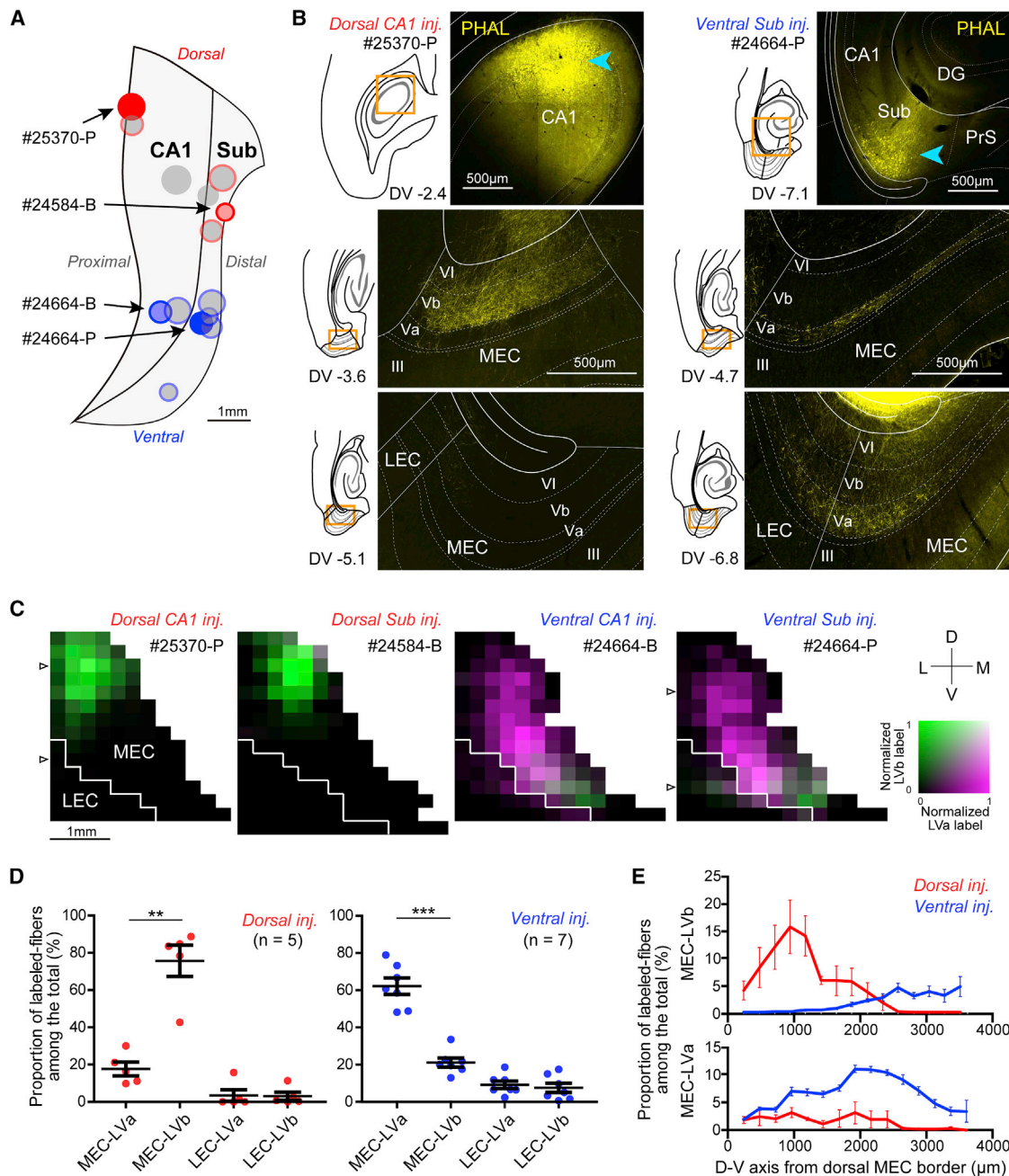
**Figure 1. Outputs from the dorsal and ventral hippocampus target different layers and dorsoventral levels of MEC in rats**

(A) Two-dimensional unfolded map of CA1 and subiculum showing the positions of anterograde tracer (PHA-L or BDA) injection sites for rat samples in the horizontal plane. Injection sites in the dorsal and ventral hippocampus are shown in red and blue, respectively.

(B) Representative samples with injection in either dorsal CA1 (left, case 25370-P) or ventral subiculum (right, case 24664-P), showing the injection site (top, cyan arrowhead) and the distribution of anterogradely labeled axons in EC at different dorsoventral (DV) levels (middle, bottom).

(C) Four representative two-dimensional density maps showing the patterns of anterogradely labeled axons in EC following anterograde tracer injections in either dorsal or ventral proximal CA1 or distal subiculum (see STAR Methods for details on how these maps were generated). Arrowheads in 25370-P and 24664-P show the positions of EC images shown in (B).

(D) Proportion of labeled fibers among all labeled fibers in MEC-LVa, MEC-LVb, LEC-LVa, and LEC-LVb for samples injected in the dorsal (red, five rats; two-tailed paired t test for MEC-LVa vs. MEC-LVb, t4 = 4.90, **p = 0.0081; LEC-LVa vs. LEC-LVb, t4 = 0.41, p = 0.70) and ventral hippocampus (blue, seven rats; two-tailed paired t test for MEC-LVa vs. MEC-LVb, t6 = 7.29, ***p = 0.0003; LEC-LVa vs. LEC-LVb, t6 = 1.07, p = 0.33).

(E) Proportion of labeled fibers in each subregion and sublayer among all labeled fibers in LVa and LVb along the dorsoventral axis of MEC for samples injected in the dorsal (red, five rats) and ventral hippocampus (blue, seven rats). Data are presented as mean ± SEM. See also Figures S2 and S3.
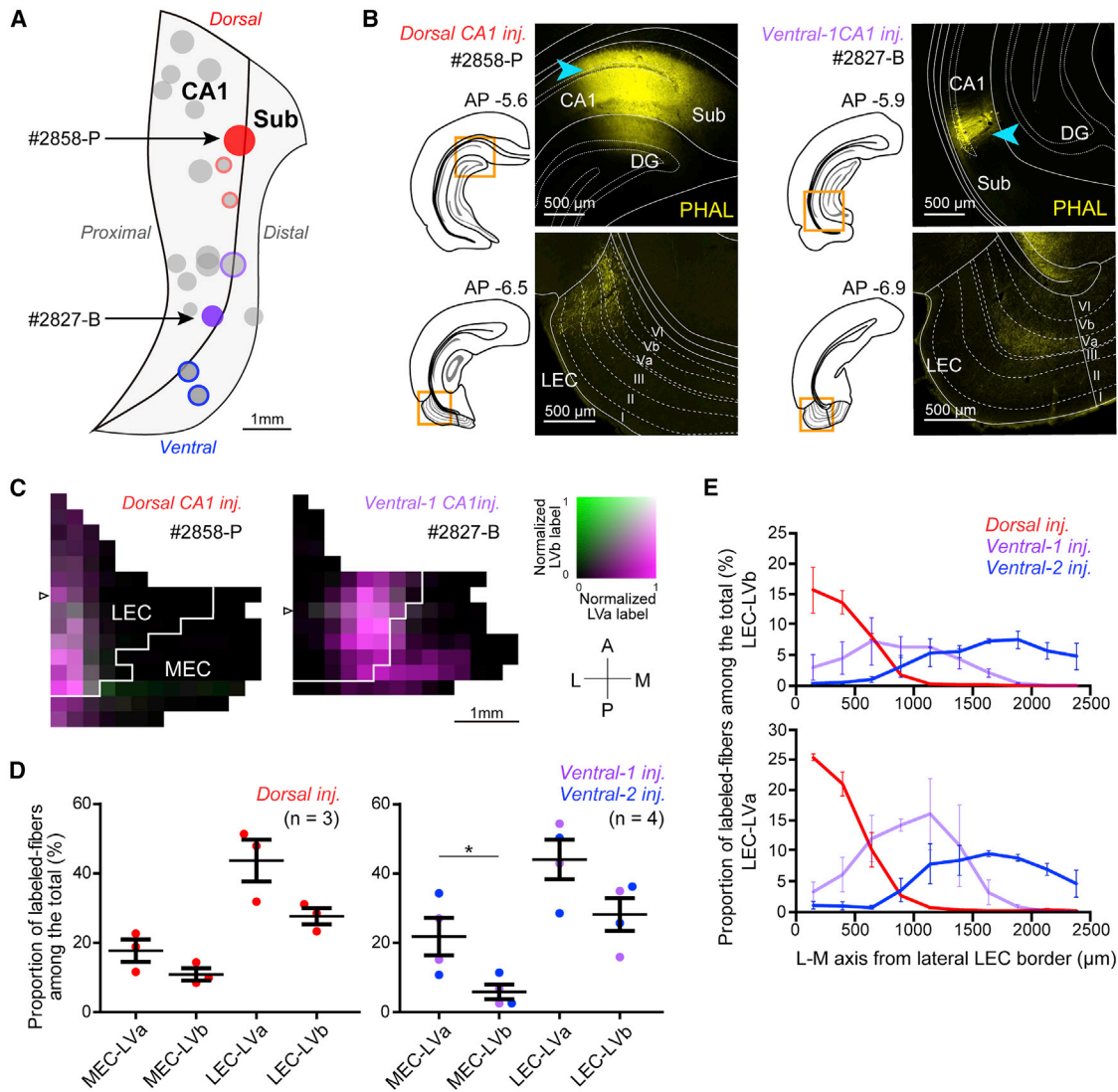
**Figure 2. Hippocampal-LEC projections are topographically organized along the dorsoventral axis**

(A) Two-dimensional unfolded map of CA1 and subiculum showing the positions of anterograde tracer (PHA-L or BDA) injection sites for rat samples in the coronal plane. Injection sites in the dorsal hippocampus are shown in red and injections into the ventral hippocampus are shown in purple (ventral-1) and blue (ventral-2).

(B) Representative samples with injection in either dorsal (left, case 2858-P) or ventral CA1 (right, case 2827-B), showing the injection site (top, cyan arrowhead) and the distribution of anterogradely labeled axons in LEC (bottom).

(C) Two-dimensional density maps showing the patterns of anterogradely labeled axons in EC. Arrowheads on the left side of the unfolded maps show the positions of LEC images shown in (B).

(D) Proportion of labeled fibers among all labeled fibers in MEC-LVa, MEC-LVb, LEC-LVa, and LEC-LVb for samples injected into the dorsal (red, three rats; two-tailed paired t test for MEC-LVa vs. MEC-LVb, t2 = 3.66, p = 0.15; LEC-LVa vs. LEC-LVb, t2 = 2.09, p = 0.28) and ventral hippocampus (purple/blue, four rats; two-tailed paired t test for MEC-LVa vs. MEC-LVb, t3 = 3.56, *p = 0.038; LEC-LVa vs. LEC-LVb, t3 = 2.01, p = 0.43).

(E) Proportion of labeled fibers in each subregion and sublayer among all labeled fibers in LVa and LVb along the dorsoventral axis of LEC for samples injected in the dorsal (red, three rats), ventral-intermediate (ventral-1, purple, two rats), and ventral hippocampus (ventral-2, blue, two rats). Data are presented as mean ± SEM. See also Figures S4 and S5.

## Hippocampal-entorhinal projections along the dorsoventral axis in mice

To examine whether the differences in hippocampal-MEC projections along the dorsoventral axis are also present in mice, we injected biotinylated dextran amine (BDA), *Phaseolus vulgaris* leukoagglutinin (PHA-L), or an adeno-associated virus (AAV) expressing synaptophysin-tagged GFP (SypGFP) and tdTomato into the mouse hippocampus. We then examined the resulting projection patterns in the sagittal plane (n = 9; Figures 3 and S6). Similar to the results in rats, projections from the dorsal hippocampus mainly terminated in dorsal MEC-LVb among the PCP4-positive neurons, used to delineate LVb (Figure 3B).[20] In contrast, projections originating from the ventral hippocampus terminated mainly in the PCP4-negative MEC-LVa. Although

the density of labeled axons was higher in ventral MEC-LVa than in dorsal MEC-LVa, axon terminals labeled by SypGFP were also observed in the dorsal tip of MEC (Figure 3B). This indicates that projections from the ventral hippocampus form synapses with LVa neurons broadly along the dorsoventral extent of MEC. In addition to labeling in LVa, labeled axons also distributed in LVb in the ventral MEC (Figures 3B and 3C). The overall hippocampal-MEC projection patterns, as seen in the mouse sagittal plane (Figure 3E), were consistent with those observed in rat horizontal (Figure 1), coronal (Figure S5), and sagittal samples (n = 6; Figure S7).

## Ventral hippocampal outputs activate LVa neurons throughout the dorsoventral axis of MEC

As described above, anatomical tracing of hippocampal outputs to MEC suggested distinct connectivity schemes for projections from the dorsal and ventral hippocampus. Whereas dorsal hippocampal outputs preferentially target LVb and to a lesser extent LVa in the dorsal half of MEC, outputs from the ventral hippocampus form a complementary pattern, targeting LVa throughout the dorsoventral extent of MEC and LVb strongly in the ventral but not dorsal MEC. To functionally test these innervation patterns, we injected an AAV expressing hChR2-EYFP under the CaMKII promoter into either the ventral or the dorsal hippocampal CA1 area (Figures S8 and S10). We then recorded excitatory postsynaptic currents (EPSCs) from both LVa and LVb excitatory neurons at four different levels of MEC, covering its entire dorsoventral extent, while activating ChR2-expressing hippocampal axons by illuminating LV with blue light (Figures 4A, 5A, S9A, and S11A). In line with the tracing experiments, injections in ventral CA1 (Figure S8) resulted in strong axonal fluorescence in LVa throughout all dorsoventral levels of MEC (Figures 4B and S9B). In LVb, strong fluorescent labeling was observed only at the two ventral section levels, with dorsal sections displaying weak to minimal fluorescence (Figures 4B and S9B). Based on this marked discrepancy in fluorescence intensity in LVb, in our initial analysis we combined the two dorsal (section levels 3 and 4) and the two ventral sections (section levels 1 and 2) for both LVa and LVb into a dorsal and ventral group, respectively. In the dorsal group, all 19 LVa and 16/19 LVb neurons exhibited short latency responses (LVa, 2.31 ms, n = 19; LVb, 2.45 ms, n = 16; p = 0.179, Mann-Whitney test) with comparable 20%–80% EPSC rise times (LVa, 1.16 ms, n = 19; LVb, 0.91 ms, n = 16; p = 0.09, Mann-Whitney test), consistent with monosynaptic input from the ventral hippocampus. One LVb cell failed to show any discernible response and two cells responded with longer latencies (median 5.13 ms), suggesting polysynaptic input to these cells. Importantly, short-latency EPSC amplitudes were significantly larger in LVa neurons compared with LVb, reaching an over 4-fold difference at higher light intensities (11.7 mW/mm$^2$, median, LVa, −0.26 nA, n = 19; LVb, −0.06 nA, n = 16; p = 0.0001, Mann-Whitney test; Figures 4C and 4D, left). To account for differences in fluorescence intensity between injections, we normalized both LVa and LVb responses to the highest LVa current amplitude at maximum light intensity in each slice. Comparison of the normalized currents revealed an even greater, roughly 5-fold difference in LVa and LVb responses across most stimulation intensities

(11.7 mW/mm$^2$, median, LVa, 1.00, n = 12; LVb, 0.20, n = 13; Figure 4D, right).

In the ventral group, all 11 LVa and 20 LVb cells responded with similarly short latencies (LVa, 2.27 ms, n = 11; LVb, 2.29 ms, n = 20; p = 0.934, Mann-Whitney test) and 20%–80% EPSC rise times (LVa, 1.07 ms, n = 11; LVb, 1.02 ms, n = 20; p = 0.664, Mann-Whitney test), confirming monosynaptic innervation by the ventral hippocampus. In contrast to the dorsal group, however, LVb responses in ventral sections were distinctly more comparable to LVa in terms of absolute (11.7 mW/mm$^2$, median, LVa, −0.41 nA, n = 11; LVb, −0.31 nA, n = 20; p = 0.223, Mann-Whitney test, Figures 4C and 4E, left) as well as normalized amplitudes, although in the latter case we did find a significant difference (11.7 mW/mm$^2$, median, LVa, 1.00, n = 10; LVb, 0.79, n = 19; Figure 4E, right).

For a more detailed characterization of hippocampal input dynamics along the dorsoventral axis of MEC, we subsequently analyzed LVa and LVb EPSC amplitudes at all four individual section levels (Figures S9A and S9B). Recordings from LVa neurons revealed strong responses at all levels of MEC with a slight but not significant trend toward smaller amplitudes in dorsal sections (11.7 mW/mm$^2$, median, level 1, −0.41 nA, n = 5; level 2, −0.38 nA, n = 6; level 3, −0.22 nA, n = 12; level 4, −0.26 nA, n = 7; Figure S9C, top) (H = 2.23; p = 0.527; p > 0.05 between all slice levels; Kruskal-Wallis test with Dunn's *post hoc* pairwise comparisons). In contrast, whereas LVb neurons also exhibited strong responses at the two ventral section levels, EPSC amplitudes in both dorsal sections were markedly lower, reaching a 6-fold difference in the dorsalmost section (11.7 mW/mm$^2$, median, level 1, −0.31 nA, n = 11; level 2, −0.31 nA, n = 9; level 3, −0.06 nA, n = 11; level 4, −0.05 nA, n = 5; Figure S9C, middle). Accordingly, statistical comparison revealed significant differences between ventral and dorsal but not the two ventral or the two dorsal section levels (H = 21.42; p < 0.001; 1 vs. 2, p > 0.05; 2 vs. 3, p < 0.05; 2 vs. 4, p < 0.05; 3 vs. 4, p > 0.05; 1 vs. 4, p < 0.01; Kruskal-Wallis test with Dunn's *post hoc* pairwise comparison). We then compared LVa and LVb responses to each other, finding them to be significantly different (F$_{(1,58)}$ = 21.04; p < 0.001; Va vs. Vb, for level 1, p = 1; for level 2, p = 1; for level 3, p = 0.008; for level 4, p = 0.007; two-way ANOVA followed by Bonferroni's *post hoc* multiple comparison test; Figure S9C, bottom). We also found differences in EPSC amplitudes through the section levels (F$_{(3,58)}$ = 10.10; p < 0.001; two-way ANOVA; Figure S9C, bottom), as well as a statistically significant interaction between slice level and EPSC amplitude of LVa and LVb neurons (F$_{(3,58)}$ = 2.89; p = 0.043; two-way ANOVA). Lastly, we examined LVb currents at individual section levels following normalization. As with absolute currents, there were no significant differences in amplitude between the two ventral or the two dorsal sections, but there was a sharp decline in EPSC amplitudes when transitioning from ventral to dorsal sections (11.7 mW/mm$^2$, median, level 1, 0.87, n = 10; level 2, 0.66, n = 9; level 3, 0.23, n = 8; level 4, 0.20, n = 5; Figure S9D) (F$_{(3,28)}$ = 14.86; p < 0.001; 1 vs. 2, p = 0.852; 2 vs. 3, p = 0.002; 2 vs. 4, p = 0.011; 3 vs. 4, p = 1.000; 1 vs. 4, p < 0.001; one-way ANOVA followed by Bonferroni's *post hoc* multiple comparison test). Together, these results corroborate findings from the anatomical tracing experiments and support a connectivity scheme where
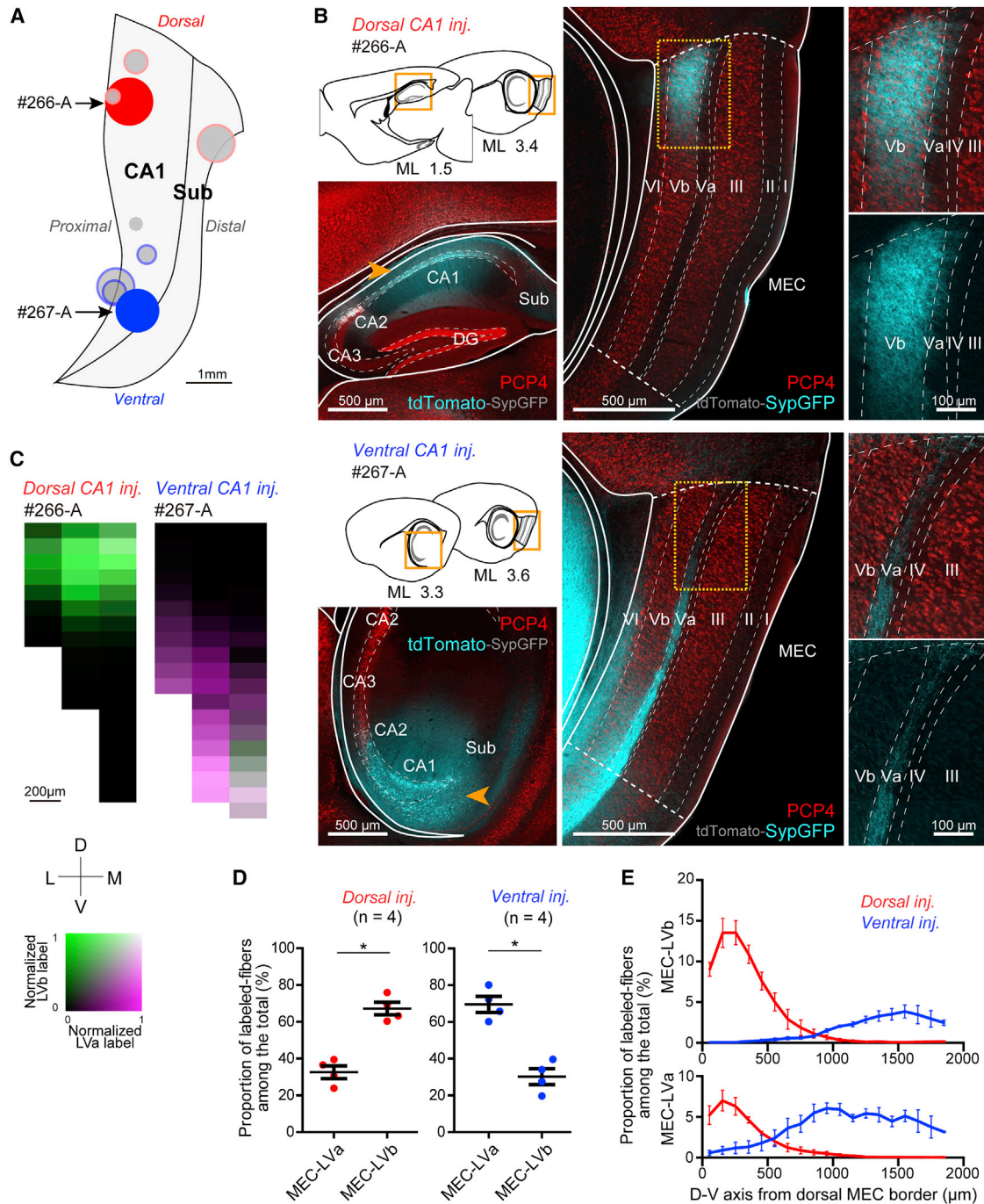
**Figure 3. Outputs from the dorsal and ventral hippocampus target different layers and dorsoventral levels of MEC in mice**

(A) Two-dimensional unfolded map of CA1 and subiculum showing the positions of anterograde tracer (PHA-L, BDA, AAV1-Syn1(S)-FLEX-tdTomato-T2A-SypGFP) injection sites for mouse samples in the sagittal plane.

(B) Representative samples with AAV injection in either dorsal (top, case 266-A) or ventral CA1 (bottom, case 267-A), showing the injection site (left, orange arrowhead) and the distribution of SypGFP-labeled axons in MEC (right). Samples are immunolabeled for PCP4 to identify the PCP4-positive layers III and Vb in MEC.

(C) Two-dimensional density maps showing the patterns of anterogradely labeled axons in MEC for the two samples shown in (B).

(D) Proportion of labeled fibers among all labeled fibers in MEC-LVa and MEC-LVb for samples injected into the dorsal (red, four mice; two-tailed paired t test, t3 = 5.03, *p = 0.015) and ventral hippocampus (blue, four mice; two-tailed paired t test, t3 = 4.56, *p = 0.020).

(E) Proportion of labeled fibers in MEC layers Va and Vb among all labeled fibers along the dorsoventral axis of MEC for samples injected into the dorsal (red, four mice) and ventral hippocampus (blue, four mice). Data are presented as mean ± SEM. See also Figures S6 and S7.
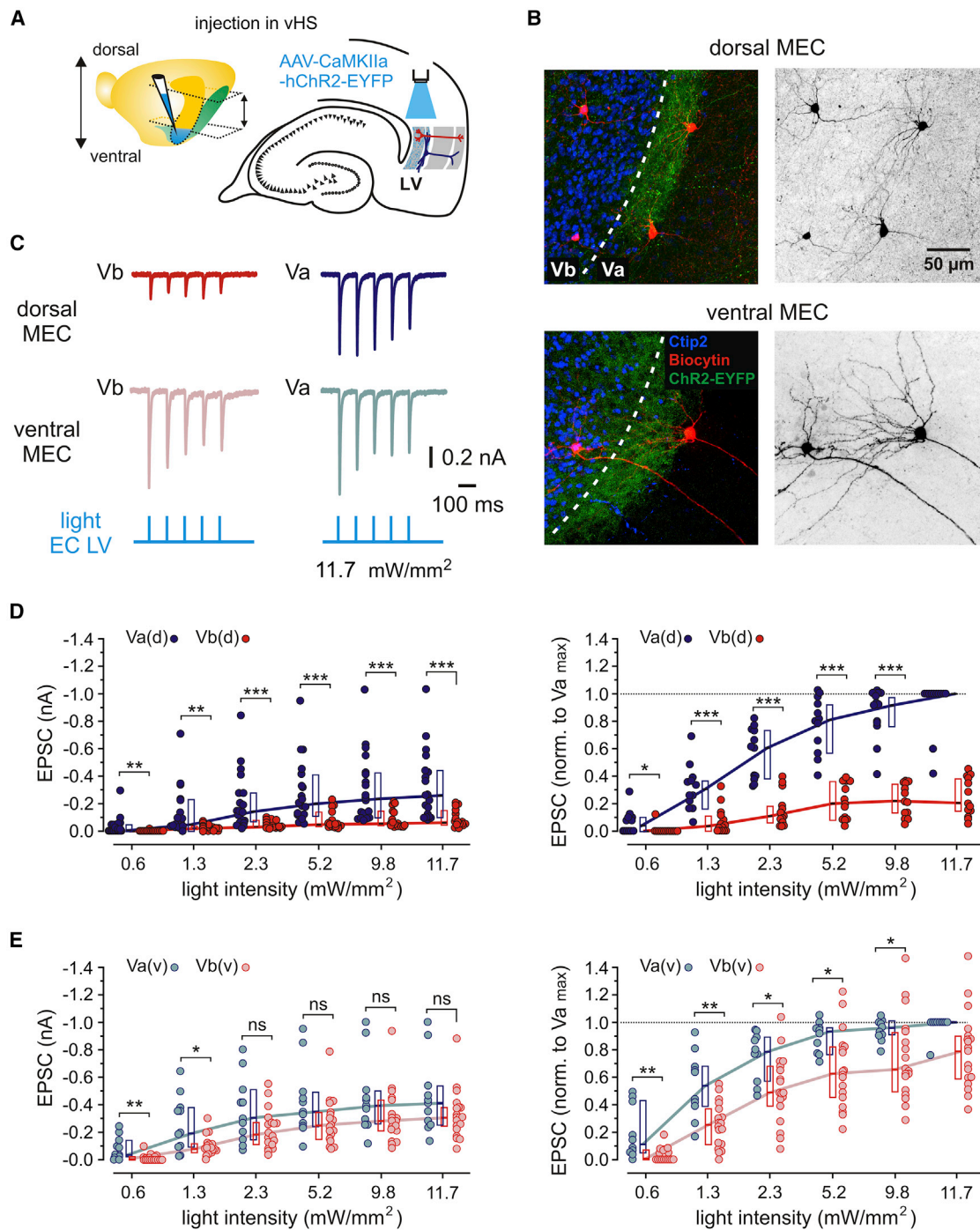
**Figure 4. Functional connectivity between the ventral hippocampus and MEC LVa and LVb excitatory neurons**

(A) Left: illustration of the injection site (blue) in the ventral hippocampus (vHS). The approximate positions of horizontal sections used in experiments are indicated by arrows. Right: schematic representation of a horizontal hippocampal-EC slice showing the position of light stimulation used to activate axons from ventral hippocampal neurons infected with AAV-CaMKIIa-hChR2-EYFP.

(B) Z-projected confocal images of biocytin-filled MEC-LVa and -LVb neurons overlaid with Ctip2 immunolabeling and fluorescent staining of hippocampal axons expressing hChR2-EYFP. The dotted line indicates the approximate border between LVb and LVa. Note the strong fluorescence of axonal fibers around Ctip2-negative LVa neurons in the dorsal MEC (top). Right images show the same neurons in black and white contrast.

(C) Example EPSC traces recorded from LVa and LVb neurons in the same slice in the dorsal (top) and ventral (middle) MEC in response to 1 ms blue light pulses (bottom).

*(legend continued on next page)*

ventral hippocampal outputs innervate LVa relatively uniformly throughout the dorsoventral extent of MEC but activate LVb with vastly different strengths between the dorsal and the ventral MEC.

### Dorsal hippocampal outputs activate LVb neurons exclusively in the dorsal MEC

We next injected AAV-hChR2-EYFP into the dorsal hippocampal CA1 area (Figure S10) and subsequently recorded from both LVa and LVb excitatory neurons at the same four MEC levels as above (Figures 5A and S11A). In agreement with the tracing experiments and consistent with previous reports,[19,20,22] we observed strong axonal fluorescence in LVb in the dorsal half of MEC (Figures 5B and S11B). We also noted individual fibers extending toward LVa (Figures 5B and S11B) as previously described.[22] Across all injections we were unable to detect any fluorescent signal in the ventral half of MEC (Figures 5B and S11B). The lack of projections from the dorsal hippocampus to the ventral MEC was confirmed by recordings from a total of 10 LVa and 9 LVb neurons at the two ventral section levels (sections 1 and 2), all of which failed to respond to light stimulation (LVa, level 1, n = 3; level 2, n = 7; LVb, level 1, n = 3; level 2, n = 6; Figures 5C, 5E, and S11C). In contrast, in the dorsal half of MEC (section levels 3 and 4) all 22 LVb and 26/34 LVa neurons responded to light stimulation with short latencies (LVb, 2.09 ms, n = 22; LVa, 1.96 ms, n = 26; p = 0.788, Mann-Whitney test) and similar 20%–80% EPSC rise times (LVb, 0.85 ms, n = 22; LVa, 0.79 ms, n = 26; p = 0.482, Mann-Whitney test), indicating monosynaptic input from the dorsal hippocampus. Of the eight remaining LVa cells, four failed to show discernible EPSCs and four responded with longer latencies (median 4.99 ms), indicative of polysynaptic input. Across most light intensities, EPSC amplitudes in LVb neurons were up to 3-fold higher than in short-latency LVa neurons (11.7 mW/mm$^2$, median, LVb, −0.55 nA, n = 22; LVa, −0.20 nA, n = 26; p = 0.0007, Mann-Whitney test, Figures 5C and 5D, left). This discrepancy in amplitudes persisted after normalizing both LVa and LVb currents to the highest LVb current amplitude at maximum light intensity in each slice, although the difference was reduced to roughly 50% across the stimulation intensities (11.7 mW/mm$^2$, median, LVb, 1.00, n = 14; LVa, 0.48, n = 12; Figure 5D, right). Analysis of EPSC amplitudes at the two dorsal section levels individually revealed that at both levels LVb neurons receive comparably strong input (11.7 mW/mm$^2$, median, level 3, −0.47 nA, n = 11; level 4, −0.56 nA, n = 11; p = 0.869, Mann-Whitney test, Figure S11C, bottom), whereas LVa responses are significantly stronger in the dorsalmost section, reaching roughly 60% of LVb amplitudes at maximum light intensity (11.7 mW/mm$^2$, median, level 3, −0.16 nA, n = 16; level 4, −0.34 nA, n = 10; p = 0.023, Mann-Whitney test, Figure S11C, top). This difference changed minimally after normalization to LVb responses, with LVa EPSCs still constituting over 50% of

LVb amplitudes at section level 4 (11.7 mW/mm$^2$, median, level 3, 0.28, n = 5; level 4, 0.54, n = 7; p = 0.034, Mann-Whitney test, Figure S11D). Based on these results, dorsal hippocampal outputs exclusively innervate the dorsal half of MEC, where they exhibit a clear preference for LVb.

## DISCUSSION

Our data reveal major differences in hippocampal-entorhinal connectivity along the dorsoventral axis of the rodent brain. By combining anatomical and electrophysiological approaches we found new, specific projection patterns from different portions of the hippocampus to both MEC and LEC. While projections to LEC maintain a strict longitudinal organization (Figure 6A), projections to MEC exhibit a hitherto unknown widespread connectivity pattern (Figure 6B). Two findings are particularly important: (1) hippocampal projections to MEC are not restricted to a single dorsoventral level; most prominently, the ventral hippocampus targets both the ventral and the dorsal MEC; (2) the specific targets of hippocampal-entorhinal projections differ along the dorsoventral axis: whereas dorsal hippocampal projections excite mainly LVb neurons in the dorsal MEC, ventral projections excite LVa neurons in both the ventral and the dorsal MEC. This architecture has strong functional implications for the transfer of information between hippocampal networks and the neocortex.

The output of patterned activity from the hippocampus to the deep layers of EC constitutes a major pathway for the transfer of information to associative neocortical networks, which likely supports the consolidation of transiently stored information into long-term memory.[26–28] At the same time, the activity patterns also propagate to superficial EC layers, from where they may return to the hippocampus, forming a recurrent feedback loop.[29–31] These two parallel pathways are associated with two different cell populations in the deep EC, namely LVa, which harbors projection neurons targeting further neocortical areas, and LVb, containing projection neurons targeting superficial EC layers.[20,32]

How the hippocampus projects to these two cell populations has remained controversial. A pioneering study on hippocampal outputs to MEC reported that projections from hippocampal CA1 selectively target LVb neurons.[19] Subsequent work showed that both LVa and LVb neurons are targeted, but the strength of innervation depends on the longitudinal position of the hippocampal origin.[22] The present study provides an account of the three-dimensional structure of the hippocampal-entorhinal output pathway. We show that neurons from ventral hippocampal levels project to both LVa and LVb in the ventral MEC but have a strong preference for LVa neurons in the dorsal MEC (Figure 6B, blue). Neurons from dorsal hippocampal portions, in contrast, project exclusively to the dorsal MEC, where they exhibit a strong preference for LVb over LVa (Figure 6B, red).

(D) Quantification of synaptic responses of LVa and LVb neurons recorded in the dorsal MEC (LVa(d), LVb(d)). Left: plots of EPSC amplitudes induced by light pulses with increasing intensities (LVa(d), 19 cells from 14 mice; LVb(d), 16 cells from 11 mice). Right: values from the left graph normalized to the highest LVa response at maximum light intensity (11.7 mW/mm$^2$) in each slice (LVa(d), 12 cells from 9 mice; LVb(d), 13 cells from 9 mice).

(E) Same analysis as in (D) for LVa and LVb neurons recorded in the ventral MEC (LVa(v), LVb(v)) (left, LVa(v), 11 cells from 8 mice; LVb(v), 20 cells from 8 mice; right, LVa(v), 10 cells from 7 mice; LVb(v), 19 cells from 7 mice). All data are presented as median, P25, and P75. Circles represent individual values. Mann-Whitney test: ***p < 0.001; **p < 0.01; *p < 0.05; ns, not significant. See also Figures S8 and S9.
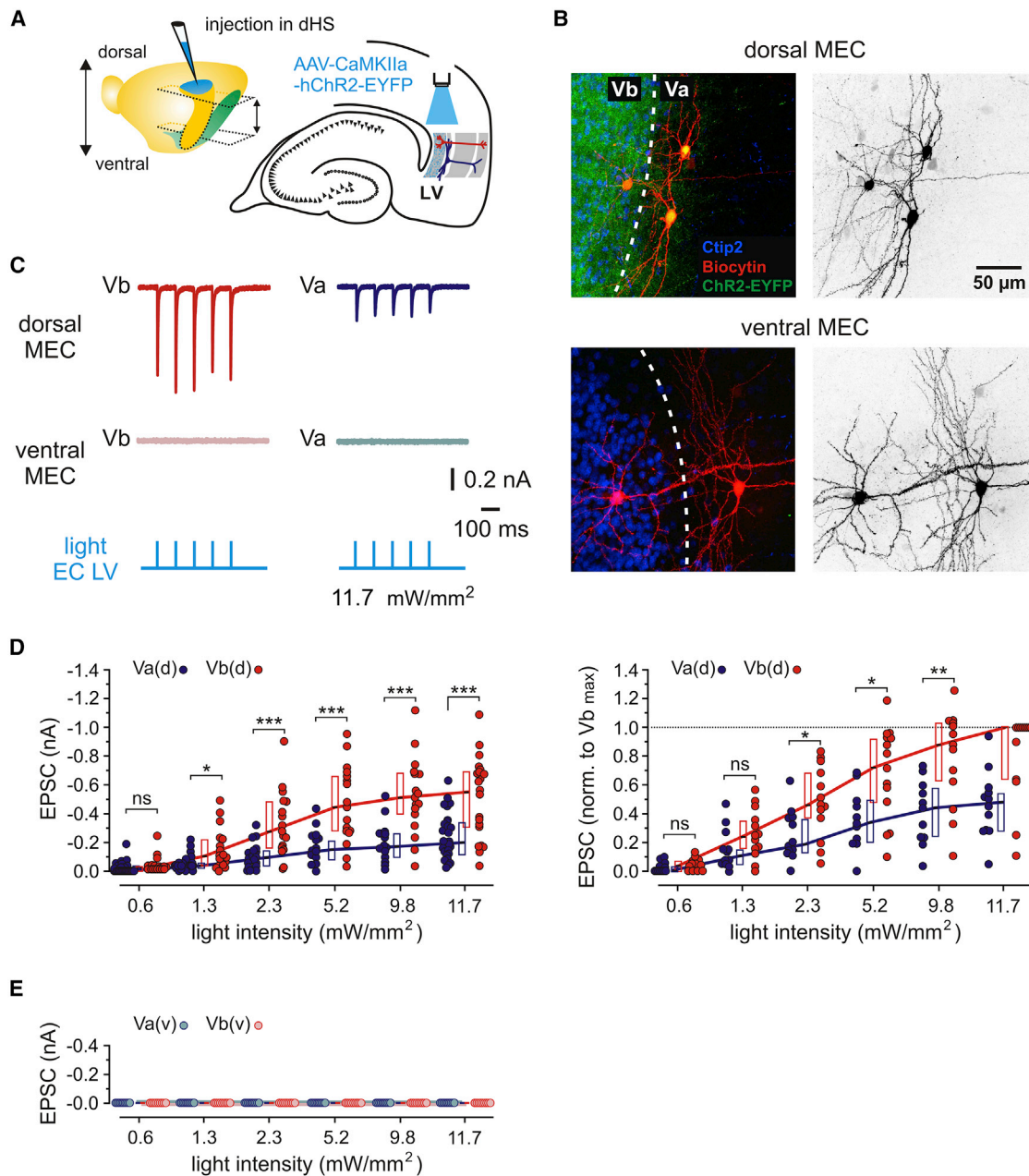
**Figure 5. Functional connectivity between the dorsal hippocampus and MEC LVa and LVb excitatory neurons**

(A) Left: illustration of the injection site (blue) in the dorsal hippocampus (dHS). The approximate positions of horizontal sections used in experiments are indicated by arrows. Right: schematic representation of a horizontal hippocampal-EC slice showing the position of light stimulation used to activate axons from dorsal hippocampal neurons infected with AAV-CaMKIIa-hChR2-EYFP.

(B) Z-projected confocal images of biocytin-filled MEC-LVa and -LVb neurons overlaid with Ctip2 immunolabeling and fluorescent staining of hippocampal axons expressing hChR2-EYFP. The dotted line indicates approximate border between LVb and LVa. Note the strong fluorescence of axonal fibers in Ctip2-positive LVb and weak but recognizable fluorescence around the Ctip2-negative LVa neuron in the dorsal MEC (top), and no fluorescence in the ventral MEC (bottom). Right images show the same neurons in black and white contrast.

(C) Example EPSC traces recorded from LVa and LVb neurons in the same slice in the dorsal (top) and ventral (middle) MEC in response to 1 ms blue light pulses (bottom).

(D) Quantification of synaptic responses of LVa and LVb neurons recorded in the dorsal MEC (LVa(d), LVb(d)). Left: plots of EPSC amplitudes induced by light pulses with increasing intensities (LVa(d), 26 cells from 14 mice; LVb(d), 22 cells from 11 mice). Right: values from the left graph normalized to the highest LVb response at maximum light intensity (11.7 mW/mm$^2$) in each slice (LVa(d), 12 cells from 7 mice; LVb(d), 14 cells from 7 mice).

(E) Same analysis as in (D) for LVa and LVb neurons recorded in the ventral MEC (LVa(v), LVb(v)) (LVa(v), 10 cells from 3 mice; LVb(v), 9 cells from 3 mice). All data are presented as median, P25, and P75. Circles represent individual values. Mann-Whitney test: ***p < 0.001; **p < 0.01; *p < 0.05; ns, not significant. See also Figures S10 and S11.
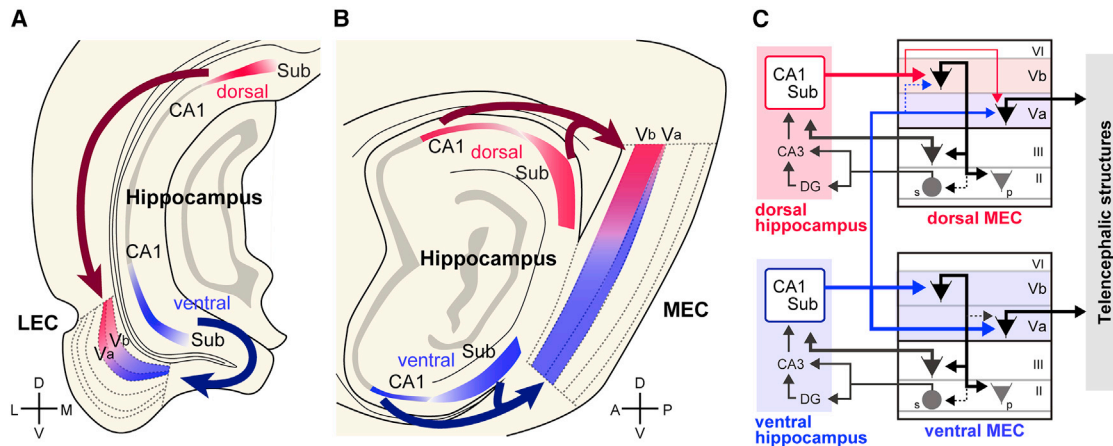
**Figure 6. Schematic diagram of hippocampal output circuits via the entorhinal cortex**
(A) Hippocampal-LEC projections are topographically organized along the dorsoventral axis.
(B) Dorsal proximal CA1/distal subiculum innervate both layer Va and layer Vb neurons in the dorsal MEC, with a marked preference for layer Vb neurons. Ventral proximal CA1/distal subiculum, in turn, innervate both layer Va and layer Vb neurons in the ventral MEC and preferentially layer Va neurons in the dorsal MEC.
(C) Information from the dorsal hippocampus is mainly sent back to the hippocampus through the MEC layer Vb → MEC layer III → hippocampus loop circuit. In contrast, information from the ventral hippocampus is sent out to telencephalic structures via the MEC layer Va output circuit. Note that dorsal hippocampal information can also reach telencephalic structures through layer Va in the dorsal MEC. s, stellate cell; p, pyramidal cell.

We found projections from ventral levels of the hippocampus to the dorsal MEC, contradicting previous anatomical studies, which reported a strict topographical organization along the dorsoventral axis, where the dorsal hippocampus projects to dorsolateral and the ventral hippocampus to ventromedial portions of EC.[12] Although our present data confirm this topographical pattern for projections to LEC, they show a much more widespread projection from the ventral hippocampus to MEC. Indeed, outputs from the ventral hippocampus reach large portions of the dorsal MEC in addition to the ventral portion. The inconsistency between our present and previous findings is likely caused by technical differences. Most previous studies examined hippocampal-entorhinal connectivity in coronally cut sections, which are unsuited for accurately evaluating labeling patterns in the dorsal MEC. This is especially the case for LVa, which in the dorsal MEC is particularly thin and can be easily overlooked in the coronal plane. Of note, one previous study did describe a dense band of terminal ventral CA1 fibers along the dorsoventral extent of MEC. This band, located in layers IV and V of the deep MEC in the nomenclature used by the authors, likely corresponds to our LVa (Figures 10D and 11B found in Cenquizca and Swanson[13]). These data are thus in line with our present findings, even though the authors supported a topographical distribution of CA1 projections as described above.

At a larger scale, the innervation of the dorsal MEC-LVa neurons by ventral hippocampal inputs is at odds with the long-postulated separation between the dorsal two-thirds and the ventral one-third of the hippocampus.[1] This notion was based on the fact that associational fibers of dentate hilus[33] and CA3[34] tend to stay within the limits of their respective dorsal-ventral portions of the hippocampal formation (for a review see Witter et al.[9]). Our present findings, however, point to a convergence of projections from the dorsal and ventral hippocampus in the dorsal MEC, allowing for the integration of this apparently segregated information before being pro-

jected to downstream telencephalic networks via LVa neurons. Whether the anatomical segregation between inputs to LVa and LVb neurons is translated into a functional segregation depends on the crosstalk between the populations.

In our previous studies, we have shown that LVb neurons in the dorsal MEC strongly innervate CA1-projecting LIII neurons but have only sparse connections to LVa.[20,22,23] These findings, together with the present results, suggest that the dorsal hippocampus primarily activates the LVb-mediated hippocampal-MEC-hippocampal loop, supporting reverberating activity patterns (Figure 6C, top). In contrast, the ventral hippocampus targets the hippocampal output circuit by innervating LVa neurons in both the dorsal and the ventral MEC, which in turn send projections to various telencephalic structures (Figure 6C, bottom). A part of this signal, however, could be transmitted back to the hippocampus, as MEC-LVa neurons were recently shown to target pyramidal neurons in the hippocampal CA1 region.[35]

The dorsal hippocampus is strongly involved in cognitive processes such as spatial, episodic, and declarative memory formation, requiring interactions with downstream neocortical areas.[2] How can this be achieved within the connectivity scheme outlined above? There are several possible routes for the transfer of information from the dorsal hippocampus to telencephalic structures. First, activity might propagate from dorsal to ventral hippocampal levels through intrinsic circuits. Indeed, there is a well-developed, longitudinally projecting synaptic network among CA1 pyramidal neurons,[36,37] from where activity can be directly routed to the medial prefrontal cortex through strong projections emerging from neurons in CA1 and subiculum.[38,39] In addition, neurons in the dorsal subiculum send strong excitatory projections to the retrosplenial cortex,[40–42] complemented by weaker long-range GABAergic projections from dorsal levels of CA1.[43]

Alternatively, and at the core of the present study, hippocampal output is fed into the entire EC-LVa output circuit. In LEC, this

output pathway is strictly topographically organized such that the dorsoventral axis of the hippocampus is precisely mapped onto the dorsoventral axis of LEC, enabling direct access to the telencephalon. In MEC, the LVa-mediated telencephalic pathway comprises two components. First, LVa neurons in the dorsal MEC receive weak monosynaptic input from the dorsal hippocampus, in line with our previous report[22] and in contrast to previous studies.[19,21] Although these inputs are markedly weaker for LVa than for LVb neurons, their presence opens the possibility of direct outputs from the dorsal hippocampus to the neocortex. Second, the present study shows that LVa neurons in the dorsal MEC receive additional inputs from the ventral hippocampus. The weaker activation of LVa in the dorsal MEC, roughly 50% of that seen in LVb, could thus potentially be compensated for by projections from the ventral hippocampus, as stimulation of ventral hippocampal terminals in the dorsal MEC quantitatively matched the "missing" ~50% of excitation in LVa. Synchronous input from both the dorsal and the ventral hippocampus to dorsal MEC-LVa would consequently equal the strength of excitation from the dorsal hippocampus to LVb, rendering the output to telencephalic or superficial entorhinal networks similarly efficient. It is currently unknown how many dorsal LVa neurons are simultaneously innervated by both dorsal and ventral parts of the hippocampus. In our electrophysiological recordings, 76% of tested LVa neurons showed monosynaptic responses to dorsal hippocampal input, and all tested LVa neurons showed monosynaptic responses to ventral input. It is therefore highly likely that a substantial fraction of dorsal MEC-LVa neurons integrate dorsal and ventral hippocampal signals.

What might be the functional relevance of the convergent dorsal and ventral hippocampal afferents in the dorsal MEC? Multiple lines of evidence show that the ventral hippocampus processes information related to emotion, stress, and motivation and is a critical hub for networks that process emotion-related learning.[2] These memory-related processes are supported by different state-dependent types of network oscillations, namely sharp wave-ripple complexes (SPW-Rs) for the output of hippocampal activity patterns to downstream areas[44,45] and theta oscillations for the coordination of network activity during acquisition of information.[46] Both patterns can propagate throughout the dorsoventral axis of the hippocampus,[47–49] supporting the integration of information from both the dorsal and the ventral portion. Maurer and Nadel[50] recently proposed that communication along the dorsoventral hippocampal axis is instrumental for the network to be able to recognize changes in context, whereby the ventral hippocampal output would signal such contextual change. The projection from the ventral hippocampus to the dorsal MEC, reported in our present study, would thus allow the dorsal MEC-LVa neocortical output pathway to contain both contextual and salience information. This mechanism may underlie the recent finding that the projection from MEC-LVa to the medial prefrontal cortex is essential for consolidating contextual fear memories.[24] In addition to emotional and contextual processing, it has been proposed that the ventral hippocampus could potentially support generalization across locations, contextual boundaries, and events.[51] The ventral hippocampal-neocortical circuit via MEC may thus contribute to context generalization of existing memories. Our anatomical data indicate that a similar ventral-hippocampus-dependent transfer of hippocampal output is unlikely to be present in the LEC-LVa output pathway. It is important to note, however, that SPW-Rs may also occur asynchronously in the dorsal and ventral hippocampus[48,52,53] and that there is significant variation in theta synchrony along the dorsoventral hippocampal axis.[54] Hippocampal activity could thus also be read out independently from the ventral or dorsal portion, supporting selective activation of emotion-related vs. neutral downstream processes.

In summary, our findings reveal differential, yet partially convergent pathways for dorsal and ventral hippocampal outputs to EC. The different cognitive, behavioral, and emotional functions of dorsal and ventral hippocampal portions are reflected in distinct connectivity to downstream networks, which are likely to excite the hippocampal feedback loop in some situations and feedforward telencephalic projections in others. At the same time, there is a complex interplay between the two pathways, supported by convergent connections and multiple excitatory loops at different levels. As a result, the complex nested hippocampal-entorhinal output network may be instrumental in the integration of emotional, spatial, and contextual as well as episodic contents. Together, these inputs may provide conditional gating of information to neocortical networks mediating long-term memory formation and storage.

### Limitations of the study

To simplify our experiments, in this study we focused on hippocampal-entorhinal projections and did not consider other circuits that may have an impact on the coordinated output of hippocampal-entorhinal circuits. For example, the strong intrinsic connections between LEC and MEC[55,56] may allow the dorsal hippocampus to innervate dorsal MEC-LVa neurons indirectly via dorsal LEC-LVa/LVb neurons. The LVa-mediated MEC-neocortical output pathway may also be regulated by specific inputs to MEC-LVa neurons from other brain areas, such as the claustrum[57] or medial septum.[20] Second, although we hypothesize that the ventral hippocampus might strongly influence the signal flow in hippocampal-MEC-neocortical circuits to facilitate long-term memory formation and storage, we did not explore this *in vivo*. It will be important for future studies to investigate this hypothesis by manipulating the activity of the ventral hippocampal-MEC circuit during/following a memory task and analyzing the resulting effects on memory consolidation.

### STAR★METHODS

Detailed methods are provided in the online version of this paper and include the following:

- KEY RESOURCES TABLE
- RESOURCE AVAILABILITY
  - Lead contact
  - Materials availability
  - Data and code availability
- EXPERIMENTAL MODEL AND SUBJECT DETAILS
- METHOD DETAILS
  - Surgical procedures and tracer/virus injections

- ○ Immunohistochemistry and imaging of neuroanatomical tracing samples
- ○ Analysis of neuroanatomical tracing samples
- ○ Preparation of mouse brain slices and recording of postsynaptic responses from LV neurons
- ○ Immunohistochemistry and imaging of recorded slices
- ○ Analysis of electrophysiological data
- ● QUANTIFICATION AND STATISTICAL ANALYSIS

**AUTHOR CONTRIBUTIONS**

S.O. collected and analyzed the anatomical data. M.R. carried out whole-cell recordings. M.R. and A.V.E. performed the electrophysiological and corresponding morphological data analysis. All authors conceptualized the study, interpreted the results, and wrote the manuscript.

**DECLARATION OF INTERESTS**

The authors declare no competing interests.

**REFERENCES**

1. Moser, M.B., and Moser, E.I. (1998). Functional differentiation in the hippocampus. Hippocampus *8*, 608–619. https://doi.org/10.1002/(SICI)1098-1063.

2. Fanselow, M.S., and Dong, H.W. (2010). Are the dorsal and ventral hippocampus functionally distinct structures? Neuron *65*, 7–19. https://doi.org/10.1016/j.neuron.2009.11.031.

3. Strange, B.A., Witter, M.P., Lein, E.S., and Moser, E.I. (2014). Functional organization of the hippocampal longitudinal axis. Nat. Rev. Neurosci. *15*, 655–669. https://doi.org/10.1038/nrn3785.

4. Jung, M.W., Wiener, S.I., and McNaughton, B.L. (1994). Comparison of spatial firing characteristics of units in dorsal and ventral Hippocampus of the rat. J. Neurosci. *14*, 7347–7356. https://doi.org/10.1523/JNEUROSCI.14-12-07347.1994.

5. Kjelstrup, K.B., Solstad, T., Brun, V.H., Hafting, T., Leutgeb, S., Witter, M.P., Moser, E.I., and Moser, M.B. (2008). Finite scale of spatial representation in the hippocampus. Science *321*, 140–143. https://doi.org/10.1126/science.1157086.

6. Hafting, T., Fyhn, M., Molden, S., Moser, M.B., and Moser, E.I. (2005). Microstructure of a spatial map in the entorhinal cortex. Nature *436*, 801–806. https://doi.org/10.1038/nature03721.

7. Brun, V.H., Solstad, T., Kjelstrup, K.B., Fyhn, M., Witter, M.P., Moser, E.I., and Moser, M.B. (2008). Progressive increase in grid scale from dorsal to ventral medial entorhinal cortex. Hippocampus *18*, 1200–1212. https://doi.org/10.1002/hipo.20504.

8. Fyhn, M., Hafting, T., Witter, M.P., Moser, E.I., and Moser, M.B. (2008). Grid cells in mice. Hippocampus *18*, 1230–1238. https://doi.org/10.1002/hipo.20472.

9. Witter, M.P., Groenewegen, H.J., Lopes da Silva, F.H., and Lohman, A.H. (1989). Functional organization of the extrinsic and intrinsic circuitry of the parahippocampal region. Prog. Neurobiol. *33*, 161–253. https://doi.org/10.1016/0301-0082(89)90009-9.

10. Dolorfo, C.L., and Amaral, D.G. (1998a). Entorhinal cortex of the rat: topographic organization of the cells of origin of the perforant path projection to the dentate gyrus. J. Comp. Neurol. *398*, 25–48.

11. van Groen, T., Miettinen, P., and Kadish, I. (2003). The entorhinal cortex of the mouse: organization of the projection to the hippocampal formation. Hippocampus *13*, 133–149. https://doi.org/10.1002/hipo.10037.

12. Kloosterman, F., Witter, M.P., and Van Haeften, T. (2003a). Topographical and laminar organization of subicular projections to the parahippocampal region of the rat. J. Comp. Neurol. *455*, 156–171. https://doi.org/10.1002/cne.10472.

13. Cenquizca, L.A., and Swanson, L.W. (2007). Spatial organization of direct hippocampal field CA1 axonal projections to the rest of the cerebral cortex. Brain Res. Rev. *56*, 1–26. https://doi.org/10.1016/j.brainresrev.2007.05.002.

14. Witter, M.P., and Amaral, D.G. (2021). The entorhinal cortex of the monkey: VI. Organization of projections from the hippocampus, subiculum, presubiculum, and parasubiculum. J. Comp. Neurol. *529*, 828–852. https://doi.org/10.1002/cne.24983.

15. Witter, M.P., Doan, T.P., Jacobsen, B., Nilssen, E.S., and Ohara, S. (2017). Architecture of the entorhinal cortex A review of entorhinal anatomy in rodents with some comparative notes. Front. Syst. Neurosci. *11*, 46. https://doi.org/10.3389/fnsys.2017.00046.

16. Kitamura, T., Pignatelli, M., Suh, J., Kohara, K., Yoshiki, A., Abe, K., and Tonegawa, S. (2014). Island cells control temporal association memory. Science *343*, 896–901. https://doi.org/10.1126/science.1244634.

17. Masurkar, A.V., Srinivas, K.V., Brann, D.H., Warren, R., Lowes, D.C., and Siegelbaum, S.A. (2017). Medial and lateral entorhinal cortex differentially excite deep versus superficial CA1 pyramidal neurons. Cell Rep. *18*, 148–160. https://doi.org/10.1016/j.celrep.2016.12.012.

18. Ramsden, H.L., Sürmeli, G., McDonagh, S.G., and Nolan, M.F. (2015). Laminar and dorsoventral molecular organization of the medial entorhinal cortex revealed by large-scale anatomical analysis of gene expression. PLoS Comput. Biol. *11*, e1004032. https://doi.org/10.1371/journal.pcbi.1004032.

19. Sürmeli, G., Marcu, D.C., McClure, C., Garden, D.L.F., Pastoll, H., and Nolan, M.F. (2015). Molecularly defined circuitry reveals input-output segregation in deep layers of the medial entorhinal cortex. Neuron *88*, 1040–1053. https://doi.org/10.1016/j.neuron.2015.10.041.

20. Ohara, S., Onodera, M., Simonsen, Ø.W., Yoshino, R., Hioki, H., Iijima, T., Tsutsui, K.I., and Witter, M.P. (2018). Intrinsic projections of layer Vb neurons to layers Va, III, and II in the lateral and medial entorhinal cortex of the rat. Cell Rep. *24*, 107–116. https://doi.org/10.1016/j.celrep.2018.06.014.

21. Wozny, C., Beed, P., Nitzan, N., Pössnecker, Y., Rost, B.R., and Schmitz, D. (2018). VGLUT2 functions as a differential marker for hippocampal output neurons. Front. Cell. Neurosci. *12*, 337. https://doi.org/10.3389/fncel.2018.00337.

22. Rozov, A., Rannap, M., Lorenz, F., Nasretdinov, A., Draguhn, A., and Egorov, A.V. (2020). Processing of hippocampal network activity in the receiver network of the medial entorhinal cortex layer V. J. Neurosci. *40*, 8413–8425. https://doi.org/10.1523/JNEUROSCI.0586-20.2020.

23. Ohara, S., Blankvoort, S., Nair, R.R., Nigro, M.J., Nilssen, E.S., Kentros, C., and Witter, M.P. (2021a). Local projections of layer Vb-to-Va are more prominent in lateral than in medial entorhinal cortex. Elife 10, 672622–e67325. https://doi.org/10.7554/eLife.67262.

24. Kitamura, T., Ogawa, S.K., Roy, D.S., Okuyama, T., Morrissey, M.D., Smith, L.M., Redondo, R.L., and Tonegawa, S. (2017). Engrams and circuits crucial for systems consolidation of a memory. Science 356, 73–78. https://doi.org/10.1126/science.aam6808.

25. Naber, P.A., Lopes Da Silva, F.H., and Witter, M.P. (2001). Reciprocal connections between the entorhinal cortex and hippocampal fields CA1 and the subiculum are in register with the projections from CA1 to the subiculum. Hippocampus 11, 99–104. https://doi.org/10.1002/hipo.1028.

26. Siapas, A.G., and Wilson, M.A. (1998). Coordinated interactions between hippocampal ripples and cortical spindles during slow-wave sleep. Neuron 21, 1123–1128. https://doi.org/10.1016/s0896-6273(00)80629-7.

27. Girardeau, G., Benchenane, K., Wiener, S.I., Buzsáki, G., and Zugaro, M.B. (2009). Selective suppression of hippocampal ripples impairs spatial memory. Nat. Neurosci. 12, 1222–1223. https://doi.org/10.1038/nn.2384.

28. Khodagholy, D., Gelinas, J.N., and Buzsáki, G. (2017). Learning-enhanced coupling between ripple oscillations in association cortices and hippocampus. Science 358, 369–372. https://doi.org/10.1126/science.aan6203.

29. Iijima, T., Witter, M.P., Ichikawa, M., Tominaga, T., Kajiwara, R., and Matsumoto, G. (1996). Entorhinal-hippocampal interactions revealed by real-time imaging. Science 272, 1176–1179. https://doi.org/10.1126/science.272.5265.1176.

30. Kloosterman, F., Van Haeften, T., Witter, M.P., and Lopes Da Silva, F.H. (2003b). Electrophysiological characterization of interlaminar entorhinal connections: an essential link for re-entrance in the hippocampal-entorhinal system. Eur. J. Neurosci. 18, 3037–3052. https://doi.org/10.1111/j.1460-9568.2003.03046.x.

31. Yamamoto, J., and Tonegawa, S. (2017). Direct medial entorhinal cortex input to hippocampal CA1 is crucial for extended quiet awake replay. Neuron 96, 217–227.e4. https://doi.org/10.1016/j.neuron.2017.09.017.

32. Ohara, S., Yoshino, R., Kimura, K., Kawamura, T., Tanabe, S., Zheng, A., Nakamura, S., Inoue, K., Takada, M., Tsutsui, K.I., and Witter, M.P. (2021b). Laminar organization of the entorhinal cortex in macaque monkeys based on cell-type-specific markers and connectivity. Front. Neural Circuits 15, 790116. https://doi.org/10.3389/fncir.2021.790116.

33. Fricke, R., and Cowan, W.M. (1978). An autoradiographic study of the commissural and ipsilateral hippocampo-dentate projections in the adult rat. J. Comp. Neurol. 181, 253–269. https://doi.org/10.1002/cne.901810204.

34. Swanson, L.W., Wyss, J.M., and Cowan, W.M. (1978). An autoradiographic study of the organization of intrahippocampal association pathways in the rat. J. Comp. Neurol. 181, 681–715. https://doi.org/10.1002/cne.901810402.

35. Tsoi, S.Y., Öncül, M., Svahn, E., Robertson, M., Bogdanowicz, Z., McClure, C., and Sürmeli, G. (2022). Telencephalic outputs from the medial entorhinal cortex are copied directly to the hippocampus. Elife 11, e73162. https://doi.org/10.7554/eLife.73162.

36. Amaral, D.G., and Witter, M.P. (1989). The three-dimensional organization of the hippocampal formation: a review of anatomical data. Neuroscience 31, 571–591. https://doi.org/10.1016/0306-4522(89)90424-7.

37. Yang, S., Yang, S., Moreira, T., Hoffman, G., Carlson, G.C., Bender, K.J., Alger, B.E., and Tang, C.M. (2014). Interlamellar CA1 network in the hippocampus. Proc. Natl. Acad. Sci. USA 111, 12919–12924. https://doi.org/10.1073/pnas.1405468111.

38. Jay, T.M., and Witter, M.P. (1991). Distribution of hippocampal CA1 and subicular efferents in the prefrontal cortex of the rat studied by means of anterograde transport of Phaseolus vulgaris-leucoagglutinin. J. Comp. Neurol. 313, 574–586. https://doi.org/10.1002/cne.903130404.

39. Hoover, W.B., and Vertes, R.P. (2007). Anatomical analysis of afferent projections to the medial prefrontal cortex in the rat. Brain Struct. Funct. 212, 149–179. https://doi.org/10.1007/s00429-007-0150-4.

40. Witter, M.P., Ostendorf, R.H., and Groenewegen, H.J. (1990). Heterogeneity in the dorsal subiculum of the rat. Distinct neuronal Zones project to different cortical and Subcortical targets. Eur. J. Neurosci. 2, 718–725. https://doi.org/10.1111/j.1460-9568.1990.tb00462.x.

41. Bienkowski, M.S., Bowman, I., Song, M.Y., Gou, L., Ard, T., Cotter, K., Zhu, M., Benavidez, N.L., Yamashita, S., Abu-Jaber, J., et al. (2018). Integration of gene expression and brain-wide connectivity reveals the multiscale organization of mouse hippocampal networks. Nat. Neurosci. 21, 1628–1643. https://doi.org/10.1038/s41593-018-0241-y.

42. Cembrowski, M.S., Phillips, M.G., DiLisio, S.F., Shields, B.C., Winnubst, J., Chandrashekar, J., Bas, E., and Spruston, N. (2018). Dissociable structural and functional hippocampal outputs via distinct subiculum cell classes. Cell 173, 1280–1292.e18. https://doi.org/10.1016/j.cell.2018.03.031.

43. Miyashita, T., and Rockland, K.S. (2007). GABAergic projections from the hippocampus to the retrosplenial cortex in the rat. Eur. J. Neurosci. 26, 1193–1204. https://doi.org/10.1111/j.1460-9568.2007.05745.x.

44. Buzsáki, G. (1986). Hippocampal sharp waves: their origin and significance. Brain Res. 398, 242–252. https://doi.org/10.1016/0006-8993(86)91483-6.

45. Buzsáki, G. (2015). Hippocampal sharp wave-ripple: a cognitive biomarker for episodic memory and planning. Hippocampus 25, 1073–1188. https://doi.org/10.1002/hipo.22488.

46. O'Keefe, J. (1993). Hippocampus, theta, and spatial memory. Curr. Opin. Neurobiol. 3, 917–924. https://doi.org/10.1016/0959-4388(93)90163-s.

47. Patel, J., Fujisawa, S., Berényi, A., Royer, S., and Buzsáki, G. (2012). Traveling theta waves along the entire septotemporal Axis of the Hippocampus. Neuron 75, 410–417. https://doi.org/10.1016/j.neuron.2012.07.015.

48. Patel, J., Schomburg, E.W., Berényi, A., Fujisawa, S., and Buzsáki, G. (2013). Local generation and propagation of ripples along the septotemporal Axis of the Hippocampus. J. Neurosci. 33, 17029–17041. https://doi.org/10.1523/JNEUROSCI.2036-13.2013.

49. Lubenov, E.V., and Siapas, A.G. (2009). Hippocampal theta oscillations are travelling waves. Nature 459, 534–539. https://doi.org/10.1038/nature08010.

50. Maurer, A.P., and Nadel, L. (2021). The continuity of context: a role for the Hippocampus. Trends Cogn. Sci. 25, 187–199. https://doi.org/10.1016/j.tics.2020.12.007.

51. Keinath, A.T., Wang, M.E., Wann, E.G., Yuan, R.K., Dudman, J.T., and Muzzio, I.A. (2014). Precise spatial coding is preserved along the longitudinal hippocampal axis. Hippocampus 24, 1533–1548. https://doi.org/10.1002/hipo.22333.

52. Sosa, M., Joo, H.R., and Frank, L.M. (2020). Dorsal and ventral hippocampal sharp-wave ripples activate distinct Nucleus accumbens networks. Neuron 105, 725–741.e8. https://doi.org/10.1016/j.neuron.2019.11.022.

53. Nitzan, N., Swanson, R., Schmitz, D., and Buzsáki, G. (2022). Brain-wide interactions during hippocampal sharp wave ripples. Proc. Natl. Acad. Sci. USA 119, e2200931119. https://doi.org/10.1073/pnas.2200931119.

54. Long, L.L., Bunce, J.G., and Chrobak, J.J. (2015). Theta variation and spatiotemporal scaling along the septotemporal axis of the hippocampus. Front. Syst. Neurosci. 9, 37. https://doi.org/10.3389/fnsys.2015.00037.

55. Dolorfo, C.L., and Amaral, D.G. (1998b). Entorhinal cortex of the rat: organization of intrinsic connections. J. Comp. Neurol. 398, 49–82. https://doi.org/10.1002/(sici)1096-9861(19980817)398:1<49::aid-cne4>3.0.co.

56. Vandrey, B., Armstrong, J., Brown, C.M., Garden, D.L.F., and Nolan, M.F. (2022). Fan cells in lateral entorhinal cortex directly influence medial entorhinal cortex through synaptic connections in layer 1. Elife. https://doi.org/10.7554/eLife.83008.

57. Kitanishi, T., and Matsuo, N. (2017). Organization of the claustrum-to-entorhinal cortical connection in mice. J. Neurosci. 37, 269–280.

58. Papp, E.A., Leergaard, T.B., Calabrese, E., Johnson, G.A., and Bjaalie, J.G. (2014). Waxholm space atlas of the Sprague Dawley rat brain. Neuroimage *97*, 374–386. https://doi.org/10.1016/j.neuroimage.2014.04.001.

59. Boccara, C.N., Kjonigsen, L.J., Hammer, I.M., Bjaalie, J.G., Leergaard, T.B., and Witter, M.P. (2015). A three-plane architectonic atlas of the rat hippocampal region. Hippocampus *25*, 838–857. https://doi.org/10.1002/hipo.22407.

60. Kjonigsen, L.J., Lillehaug, S., Bjaalie, J.G., Witter, M.P., and Leergaard, T.B. (2015). Waxholm Space atlas of the rat brain hippocampal region: three-dimensional delineations based on magnetic resonance and diffusion tensor imaging. Neuroimage *108*, 441–449. https://doi.org/10.1016/j.neuroimage.2014.12.080.

61. Swanson, L.W., and Hahn, J.D. (2020). A qualitative solution with quantitative potential for the mouse hippocampal cortex flatmap problem. Proc. Natl. Acad. Sci. USA *117*, 3220–3231. https://doi.org/10.1073/pnas.1918907117.

62. Roth, F.C., Beyer, K.M., Both, M., Draguhn, A., and Egorov, A.V. (2016). Downstream effects of hippocampal sharp wave ripple oscillations on medial entorhinal cortex layer V neurons in vitro. Hippocampus *26*, 1493–1508. https://doi.org/10.1002/hipo.22623.

63. Viana da Silva, S., Zhang, P., Haberl, M.G., Labrousse, V., Grosjean, N., Blanchet, C., Frick, A., and Mulle, C. (2019). Hippocampal mossy fibers synapses in CA3 pyramidal cells are altered at an early stage in a mouse model of alzheimer's disease. J. Neurosci. *39*, 4193–4205. https://doi.org/10.1523/JNEUROSCI.2868-18.2019.

## STAR★METHODS

### KEY RESOURCES TABLE

| REAGENT or RESOURCE | SOURCE | IDENTIFIER |
| --- | --- | --- |
| **Antibodies** | | |
| Rat anti-Ctip2 | Abcam | Cat# ab18465; RRID:AB_2064130 |
| Cy3-conjugated anti-rat | Jackson ImmunoResearch | Cat# 112-165-003; RRID:AB_2338240 |
| Streptavidin-conjugated Alexa Fluor 546 | Invitrogen | Cat# S11225; RRID:AB_2532130 |
| Alexa Fluor 647 anti-rat | Invitrogen | Cat# A21247; RRID:AB_141778 |
| Rabbit anti-PHA-L | Vector Laboratories | Cat# AS-2300; RRID:AB_2313686 |
| Mouse anti-GFP | Invitrogen | Cat# A11120; RRID:AB_221568 |
| Guinea pig anti-NeuN | Millipore | Cat# ABN90P; RRID:AB_2341095 |
| Mouse anti-NeuN | Millipore | Cat# MAB377; RRID:AB_2298772 |
| Rabbit anti-PCP4 | Sigma Aldrich | Cat# HPA005792; RRID:AB_1855086 |
| Cy3-Streptavidin | Jackson ImmunoResearch | Cat# 016-160-084; RRID:AB_2337244 |
| Alexa Fluor 647 goat anti-rabbit IgG | Jackson ImmunoResearch | Cat# 111-605-144; RRID:AB_2338078 |
| Cy3 goat anti-mouse IgG | Jackson ImmunoResearch | Cat# 115-165-146; RRID:AB_2338690 |
| Alexa Fluor 647 goat anti-guinea pig IgG | Jackson ImmunoResearch | Cat# 106-605-003; RRID:AB_2337446 |
| Alexa Fluor 647 goat anti-mouse IgG | Jackson ImmunoResearch | Cat# 115-605-003; RRID:AB_2338902 |
| **Bacterial and virus strains** | | |
| AAV5-CaMKIIa-hChR2(H134R)-EYFP | UNC vector core | Karl Deisseroth virus stock |
| AAV5-CaMKIIa-hChR2(H134R)-EYFP | Addgene | Cat# 26969-AAV5 |
| AAV1-Syn1(S)-FLEX-tdTomato-T2A-SypEGFP | Addgene | Cat# 51509-AAV1 |
| AAV9.CaMKII 0.4.Cre | Addgene | Cat# 105558-AAV9 |
| **Chemicals, peptides, and recombinant proteins** | | |
| Biotinylated dextran amine | Invitrogen | Cat# D1956; RRID:AB_2307337 |
| Phaseolus vulgaris leucoagglutinin | Vector Laboratories | Cat# L-1110; RRID:AB_2336656 |
| Biocytin | Sigma-Aldrich | Cat# B4261 |
| DAPI | Carl Roth | Cat# 6335.1 |
| **Experimental models: Organisms/strains** | | |
| Mice C57BL/6N | Charles River<br>Japan SLC | Strain code: 027<br>010203 |
| Sprague-Dawley rat | Japan SLC | 020101 |
| **Software and algorithms** | | |
| CorelDRAW | Corel Corporation | X4 |
| ImageJ/Fiji | NIH | https://imagej.net/Fiji; RRID:SCR_002285 |
| GraphPad | InStat | V3.10 http://graphpad.com/; RRID:SCR_000306 |
| Matlab | The Mathworks, Inc | https://www.mathworks.com/; RRID: SCR_001622 |
| SigmaPlot | Systat | V11.0 http://www.sigmaplot.com/products/sigmaplot/; RRID:SCR_003210 |
| Origin | OriginLab | Origin 7G; http://microcal-origin.software.informer.com/; RRID:SCR_002815 |

## RESOURCE AVAILABILITY

### Lead contact
Further information and requests for resources and reagents should be directed to and will be fulfilled by the lead contact, Menno Witter (menno.witter@ntnu.no).

### Materials availability
This study did not generate new unique reagents.

### Data and code availability
- Data will be available from the lead contact upon request.
- This paper does not report original code.
- Any additional information required to reanalyze the data reported in this paper is available from the lead contact upon request.

## EXPERIMENTAL MODEL AND SUBJECT DETAILS

Projection patterns from the hippocampus to EC were anatomically characterized using adult male C57BL/6N mice (n = 6), adult male SD rats (n = 4) and adult female SD rats (n = 19). Predicted connectivity was electrophysiologically verified using brain slices obtained from 10 to 12 week old male C57BL/6N mice (n = 40). Mice and rats were purchased from Japan SLC (Shizuoka, Japan) or Charles River Laboratories (Sulzfeld, Germany). Animals were group housed at a 12:12 h reversed day/night cycle and had ad libitum access to food and water. All experiments were approved either by the Center for Laboratory Animal Research, Tohoku University (Projects: 2017LsA-017; 2017LsA-018), the state government of Baden-Württemberg (Projects: G206/20; G58/21), or by the Norwegian Animal Research Authority (Project: #8082). The experiments were conducted in accordance with the Tohoku University Guidelines for Animal Care and Use, German law, the European Communities Council Directive and the Norwegian Experiments on Animals Act.

## METHOD DETAILS

### Surgical procedures and tracer/virus injections
For the *in vivo* delivery of tracers or viral vectors, animals were deeply anesthetized with vaporized isoflurane and mounted in a stereotaxic frame. Anesthesia was maintained throughout the operation by mask inhalation of isoflurane at concentrations between 1.5 and 2.5%. Animals used for anatomical experiments were injected subcutaneously with buprenorphine hydrochloride (0.1 mg/kg, Temgesic, Indivior), meloxicam (1 mg/kg, Metacam Boehringer Ingelheim Vetmedica), and at the incision site with bupivacaine hydrochloride (Marcain 1 mg/kg, Astra Zeneca). Mice used for electrophysiological experiments were injected with buprenorphine (0.1 mg/kg, s.c.) 30 min before and 3 h after each surgery. Following head fixation, the skull was exposed and a small burr hole was drilled above the injection site. For anterograde tracing experiments, either 2.5% phaseolus vulgaris leucoagglutinin (PHA-L; Vector Laboratories, #L-1110) or 3.5–5.0% 10 kDa biotinylated dextran amine (BDA; Invitrogen, #D1956) was injected iontophoretically with positive 6–12 mA current pulses (6 s on, 6 s off) for 15 min. Alternatively, an adeno-associated virus (AAV) cocktail was used, consisting of AAV1-Syn1(S)-FLEX-tdTomato-T2A-SypEGFP ($1.8 \times 10^{13}$ GC/mL, 133 nL, Addgene #51509) and AAV9.CaMKII 0.4.Cre ($2.1 \times 10^{13}$ GC/mL, 67 nL, Addgene #105558), 200 nL of which was pressure injected using a glass micropipette (outer tip diameter = 20–40 $\mu$m) connected to a 1 $\mu$L Hamilton microsyringe. For electrophysiological experiments, 70–100 nL of AAV5-CaMKIIa-hChR2(H134R)-EYFP (UNC vector core, Karl Deisseroth virus stock/Addgene #26969) was injected unilaterally into either the ventral (AP = $-2.8 - -3.1$ mm; ML = $\pm 3.4$ mm; DV = $-4.0$ mm (21 mice)) or the dorsal hippocampus (AP = $-2$ mm; ML = $\pm 2$ mm; DV = $-1.5$ mm (10 mice) or AP = $-1.5$ mm; ML = $\pm 1.2$ mm; DV = $-1.4$ mm (9 mice)) at a rate of 200 nL per minute using a stainless steel needle (NF33BV, inner tip diameter = 115 $\mu$m) connected to a 10 $\mu$L NanoFil Syringe (WPI, Sarasota, USA). Following each injection, the pipette was left in place for another 10–15 min before being withdrawn. The wound was sutured and the animal was monitored for recovery from anesthesia, after which it was returned to its home cage.

### Immunohistochemistry and imaging of neuroanatomical tracing samples
Ten days after tracer or 3–4 weeks after viral injections the injected animals were anesthetized with isoflurane, euthanized with a lethal intraperitoneal injection of pentobarbital (100 mg/kg), and subsequently transcardially perfused, first with Ringer's solution (0.85% NaCl, 0.025% KCl, 0.02% NaHCO3) and then with 4% paraformaldehyde (PFA) in 0.1 M phosphate buffer (PB). Brains were removed from the skull, post-fixed in PFA overnight, and put in a cryo-protective solution containing 20% glycerol and 2% dimethylsulfoxid (DMSO) diluted in 0.125 M PB. A freezing microtome was used to cut the brains into 40-$\mu$m-thick sections in either the coronal, horizontal, or sagittal plane, which were collected in six equally spaced series for processing.

To visualize PHA-L, sections were stained with primary (1:1000, rabbit anti-PHA-L, Vector Laboratories AS-2300) and secondary antibodies (1:400, Alexa Fluor 647 goat anti-rabbit IgG, Jackson ImmunoResearch #111-605-144), while BDA was visualized with Cy3-streptavidin (1:400, Jackson ImmunoResearch #016-160-084). GFP signal was enhanced with a primary (1:500, mouse

anti-GFP, Invitrogen #A11120) and secondary antibody (1:400, Cy3 goat anti-mouse IgG, Jackson ImmunoResearch #115-165-146). For delineation purposes, sections were stained with primary (1:1000, guinea pig anti-NeuN, Millipore #ABN90P; 1:1000, mouse anti-NeuN, Millipore #MAB377; 1:300, rabbit anti-PCP4, Sigma Aldrich #HPA005792) and secondary antibodies (Alexa Fluor 647 goat anti-guinea pig IgG, Jackson ImmunoResearch #106-605-003; Alexa Fluor 647 goat anti-mouse IgG, Jackson ImmunoResearch #115-605-003; Alexa Fluor 647 goat anti-rabbit IgG).

For immunofluorescence staining, floating sections were rinsed in phosphate buffered saline (PBS) containing 0.1% Triton X-100 (PBS-Tx), followed by a 60 min incubation in blocking solution containing 5% goat serum in PBS-Tx at room temperature (RT). Sections were subsequently incubated with primary antibodies diluted in the blocking solution for 20–40 h at 4°C, washed in PBS-Tx (3 × 10 min), and incubated with secondary antibodies diluted in PBS-Tx for 4–6 h at RT. Finally, sections were washed in PBS (3 × 10 min), mounted on gelatin-coated slides, and coverslipped with Entellan new (Merck Chemicals, #107961).

Sections were imaged using an automated scanner (Zeiss Axio Scan Z1). In order to precisely identify the location of the injection site in horizontally or sagittally sectioned samples, we identified the corresponding location of the injection site in the coronal plane using either the Waxholm space three-plane architectonic atlas of the rat hippocampal region[58–60] or Allen Brain explorer (http://connectivity.brain-map.org/3d-viewer). To summarize the locations of the injection sites, all injection sites were transferred from the coronal plots onto an unfolded template map of CA1 and subiculum.[61]

### Analysis of neuroanatomical tracing samples

The distribution of labeled axons in EC layer V was quantified either in coronal, horizontal, or sagittal sections spaced 240 μm apart. After identifying MEC and LEC and their respective layers,[20,23] EC was divided into columnar bins by first dividing layer IV into 100–200 μm-wide bins and then extending the columnar bin to layers Va and Vb (Figure S1, step 1). Fluorescence intensity of immunohistochemically labeled axons within each bin was quantified using ImageJ/Fiji (Wayne Rasband, NIH, USA, open source). The intensity of immunolabeling in all bins was normalized to the bin with maximum intensity in the same sample and the normalized intensities were plotted on an unfolded map of EC layer Va/Vb as a grayscale image (Figure S1, step 2). We further created a composite image of these two grayscale maps of LVa and LVb using the "falsecolor" method in MATLAB (MathWorks, USA; Figure S1, step 3). This method allows to visualize the differences in labeling patterns between LVa and LVb in different color bands, green and magenta. Green indicates bins with higher label intensity in LVb than LVa, and magenta indicates bins with higher label intensity in LVa than LVb. Bins where LVa and LVb have the same intensity are shown in gray.

To compare the differences in hippocampal projection patterns between MEC-LVa, MEC-LVb, LEC-LVa, and LEC-LVb, we summed up the normalized fluorescence intensities of bins within each subregion/layer. The proportion of labeled fibers in MEC-LVa/MEC-LVb/LEC-LVa/LEC-LVb among all labeled fibers was calculated and the differences between LVa and LVb groups were tested using paired t tests.

### Preparation of mouse brain slices and recording of postsynaptic responses from LV neurons

Horizontal brain slices containing the hippocampus and entorhinal cortex were obtained a minimum of two weeks after virus injections using standard proceedings.[62] Briefly, mice were sacrificed under deep $CO_2$-induced anesthesia. After decapitation, brains were rapidly removed and placed in an ice-cold oxygenated cutting solution containing (in mM): 140 K-gluconate, 15 Na-gluconate, 4 NaCl, 10 HEPES, 0.2 EGTA, saturated with carbogen (95% $O_2$ and 5% $CO_2$, pH 7.3). 350-μm-thick horizontal slices were cut using a vibratome slicer (Leica VT1200S, Nussloch, Germany). After cutting, the slices were incubated for 20 min at ∼34°C in a lowered sodium resting solution containing (in mM): 110 NaCl, 2.5 KCl, 0.8 $CaCl_2$, 8 $MgCl_2$, 1.25 $NaH_2PO_4$, 26 $NaHCO_3$, 0.4 ascorbate, 3 pyruvate, 14 glucose (pH 7.3),[63] and subsequently stored at RT in carbogen-saturated artificial cerebrospinal fluid (ACSF) containing (in mM): 124 NaCl, 3 KCl, 1.6 $CaCl_2$, 1.8 $MgSO_4$, 10 glucose, 1.25 $NaH_2PO_4$, 26 $NaHCO_3$ (pH 7.4 at 34°C). Slices were allowed to recover for at least 1 h before the start of electrophysiological recordings.

Individual slices were then transferred to a recording chamber which was continuously superfused with oxygenated ACSF maintained at 32 ± 1°C. Layer Va and Vb excitatory neurons were identified with an upright microscope (BX-51 WI, Olympus, Japan) at 40× magnification using infrared-differential interference contrast (IR-DIC) microscopy. Whole-cell patch-clamp recordings were performed using borosilicate glass pipettes with a resistance of 4–6 MΩ filled with a K-based intracellular solution containing (in mM): 126 K-gluconate, 4 KCl, 10 HEPES, 0.3 EGTA, 4 Mg-ATP, 0.3 Na-GTP, 10 $Na_2$-phosphocreatine (pH 7.3, KOH, calculated liquid junction potential −15 mV). Axonal fibers of hippocampal pyramidal cells expressing ChR2 were excited through a 40x/0.8-NA objective using a TTL-controlled blue LED (470 nm, ThorLabs no. M470L3). Light intensity was increased at regular intervals (as indicated in Figures 4, 5, S9, and S11) and at each intensity a 10 Hz train of five 1 ms pulses was repeated three times. Light-evoked excitatory postsynaptic currents (EPSCs) were recorded in voltage-clamp mode at a holding potential of −70 mV. Whole-cell series resistance (typically between 20 and 40 MΩ) was not compensated and closely monitored during recordings. Recordings showing a change of >20% were discarded. Data were acquired using the ELC-03XS amplifier (npi electronics, Tamm, Germany) connected to an analog-to-digital converter (POWER 1401 mkII, CED, Cambridge, UK) and stored for offline analysis using Signal4 and Spike2 (v7) software (CED, Cambridge, UK). Currents were low-pass filtered at 8 kHz and digitized at 20 kHz.

Layer Va and Vb excitatory neurons were preliminarily identified based on their location, shape of cell body and firing properties as previously described.[22] During recordings, cells were filled with biocytin (1–5%, Sigma-Aldrich, Taufkirchen, Germany, Cat. No. B4261) which was later immunolabeled to determine cell morphology and location. In total, 67/74 MEC-LVa and 64/70 MEC-LVb

neurons were confirmed morphologically, while the remaining cells were defined by location only. The exact location of neurons within layer V was further verified by immunolabeling for the transcription factor Ctip2, which marks neurons in a region corresponding to sublayer Vb.

### Immunohistochemistry and imaging of recorded slices

Slices containing biocytin-filled cells were fixed in 4% PFA in PB for 45–60 min at RT and stored in PBS (pH 7.4) at 4°C. For staining, slices were pretreated in blocking solution (5% goat serum and 0.3% Triton X-100 in PBS) for 2 h at RT, followed by washing in PBS (3 × 15 min) and an overnight incubation (>16 h at RT) with the primary antibody (1:1000, rat anti-Ctip2, Abcam #ab18465) diluted in antibody solution (1% goat serum and 0.2% Triton X-100 in PBS). The next day, slices were washed in PBS (3 × 15 min) and treated with the secondary antibody (streptavidin-conjugated Alexa Fluor 546 (1:1000, Invitrogen #S11225) and Alexa Fluor 647 (1:1000, anti-rat, Invitrogen #A21247)) or with Cy3-conjugated anti-rat (1:500; 112–165-003, Jackson ImmunoResearch) in the antibody solution for 2 h at RT. Slices were then washed in PBS (3 × 15 min) and incubated with 4,6-diamidino-2-phenylindole (DAPI; 1:10,000, Carl Roth, Germany) for 2 min at RT. Finally, slices were rinsed in PBS and embedded in Mowiol 4–88 (Sigma-Aldrich, Taufkirchen, Germany). Confocal image stacks were collected with a C2 Nikon confocal microscope (Nikon Imaging Center at Heidelberg University) at 2048x2048 pixel resolution (1 $\mu$m z-steps) using 4x (0.13 NA), 10x (0.45 NA) or 20x (0.75 NA) objectives in air. Multiple confocal images were merged as maximum intensity projections and analyzed with ImageJ/Fiji.

### Analysis of electrophysiological data

Offline data analysis was performed manually on raw traces using Signal4 and Spike2 (v7). All quantified parameters were measured using the first light-evoked EPSC of individual five-pulse-trains averaged across the three repetitions. Amplitudes were defined as the difference between EPSC peak and event-free baseline before EPSC onset, which were measured by manually placing horizontal cursors. Latency values represent the time interval between the onset of light pulse and the onset of EPSC, defined as the point where the current trace shifted >5 pA from the baseline at the start of the EPSC rising phase. Latencies and 20–80% rise times were measured at maximum light intensity. When held at −70 mV, cells with a holding current >300 pA or series resistance >40 MΩ were discarded from analysis. Because no significant differences in light-evoked EPSC amplitudes between the caudal and rostral dorsal hippocampal injection locations were detected, data from both groups were pooled.

### QUANTIFICATION AND STATISTICAL ANALYSIS

For anatomical experiments, statistical analyses were performed using GraphPad Prism (GraphPad Software). Differences between LVa and LVb groups were tested using paired t tests. All statistical tests were two-tailed with thresholds for significance placed at *p < 0.05, **p < 0.01, and ***p < 0.001. All data are presented as mean ± SEM, and n represents the number of animals. Full details of statistical tests in individual figures are described in the figure legends.

For electrophysiological experiments, quantitative data from multiple slices are given as median, where n represents the number of cells. Data in figures are presented as medians, 25th, 75th percentile [P25; P75] and individual values. Statistical analysis was performed using GraphPad software (InStat, San Diego, USA) or SigmaPlot (Systat, USA). Mann-Whitney U test was used for statistical comparisons of two groups. One-way or two-way ANOVA followed by Bonferroni's post hoc test were used for statistical comparisons of multiple groups with normal distributions. Kruskal-Wallis Test (non-parametric ANOVA) followed by Dunn's post hoc pairwise comparisons was used to compare multiple groups with non-normal distributions. For two-way ANOVA data were *log10-transformed* to normal distribution.Thresholds for significance were set identically to neuroanatomical data (ns, not significant). Statistical details for individual experiments can be found in Results and respective figure legends.

Experimenters were not blind to experimental groups. No pre-test analyses were used to estimate sample sizes, but the number of mice and cells for each experiment is similar to previous studies in the field.[19,22,23] Animals were selected from different litters, and all experiments were successfully replicated in several samples.